

AD-A168 523

A MONTE CARLO DESCRIPTION OF THE SAMPLING OF
STRATOSPHERIC ION CLUSTERS V. (U) SPECTRAL SCIENCES INC
BURLINGTON MA J B ELGIN ET AL. OCT 85 SSI-TR-89

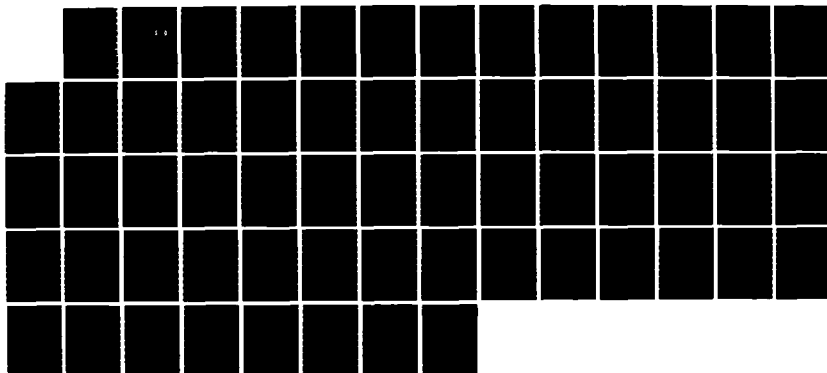
1/1

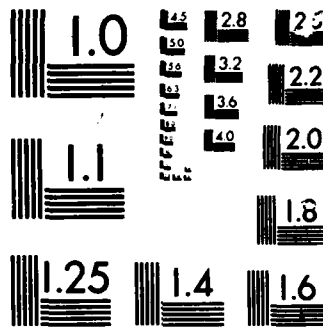
UNCLASSIFIED

AFGL-TR-85-0319 F19628-82-C-0048

F/G 4/1

NL





MICRON

CHART

AD-A168 523

AFGL-TR-85-0319

A MONTE CARLO DESCRIPTION OF THE SAMPLING OF
STRATOSPHERIC ION CLUSTERS VIA A MASS SPECTROMETER

James B. Elgin
James W. Duff

Spectral Sciences, Inc
111 S. Bedford Street
Burlington, MA 01803

October 1985

Final Report
26 January 1983 - 30 September 1985

APPROVED FOR PUBLIC RELEASE; DISTRIBUTION UNLIMITED

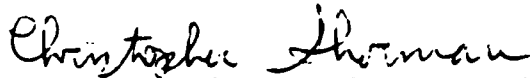
AIR FORCE GEOPHYSICS LABORATORY
AIR FORCE SYSTEMS COMMAND
UNITED STATES AIR FORCE
HANSOM AIR FORCE BASE, MASSACHUSETTS 01731

DTIC
ELECTE
JUN 06 1986
S D

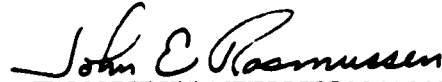
DTIC FILE COPY

86 6 6 01/8

"This technical report has been reviewed and is approved for publication"

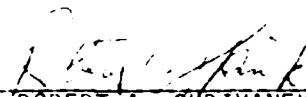


CHRISTOPHER SHERMAN
Contract Manager
Ionospheric Interactions Branch



JONH E. RASMUSSEN, Chief
Ionospheric Interactions Branch
Ionospheric Physics Division

FOR THE COMMANDER



ROBERT A. SKRIVANEK
Director
Ionospheric Physics Division

This report has been reviewed by the ESD Public Affairs Office (PA) and is releasable to the National Technical Information Service (NTIS).

Qualified requestors may obtain additional copies from the Defense Technical Information Center. All others should apply to the National Technical Information Service.

If your address has changed, or if you wish to be removed from the mailing list, or if the addressee is no longer employed by your organization, please notify AFGL/DAA, Hanscom AFB, MA 01731. This will assist us in maintaining a current mailing list.

REPORT DOCUMENTATION PAGE

1a. REPORT SECURITY CLASSIFICATION Unclassified			1b. RESTRICTIVE MARKINGS		
2a. SECURITY CLASSIFICATION AUTHORITY			3. DISTRIBUTION/AVAILABILITY OF REPORT Approved for public release; Distribution unlimited.		
2b. DECLASSIFICATION/DOWNGRADING SCHEDULE					
4. PERFORMING ORGANIZATION REPORT NUMBER(S) SSI-TR-89			5. MONITORING ORGANIZATION REPORT NUMBER(S) AFGL-TR-85-0319		
6a. NAME OF PERFORMING ORGANIZATION Spectral Sciences, Inc		6b. OFFICE SYMBOL (If applicable)	7a. NAME OF MONITORING ORGANIZATION Air Force Geophysics Laboratory		
6c. ADDRESS (City, State, and ZIP Code) 111 S. Bedford Street Burlington, MA 01803			7b. ADDRESS (City, State, and ZIP Code) Hanscom AFB Massachusetts 01731		
8a. NAME OF FUNDING/SPONSORING ORGANIZATION		8b. OFFICE SYMBOL (If applicable)	9. PROCUREMENT INSTRUMENT IDENTIFICATION NUMBER F19628-82-C-0048		
8c. ADDRESS (City, State, and ZIP Code)			10. SOURCE OF FUNDING NUMBERS		
			PROGRAM ELEMENT NO. 62101F	PROJECT NO. 6687	TASK NO. 03
11. TITLE (Include Security Classification) A Monte Carlo Description of the Sampling of Stratospheric Ion Clusters Via a Mass Spectrometer					
12. PERSONAL AUTHOR(S) James B. Elgin; James W. Duff					
13a. TYPE OF REPORT FINAL REPORT		13b. TIME COVERED FROM 1/26/83 TO 9/30/85		14. DATE OF REPORT (Year, Month, Day) October 1985	
15. PAGE COUNT 62					
16. SUPPLEMENTARY NOTATION					
17. COSATI CODES			18. SUBJECT TERMS (Continue on reverse if necessary and identify by block number)		
FIELD	GROUP	SUB-GROUP	Ion Clustering; Stratosphere; Mass Spectrometer		
19. ABSTRACT (Continue on reverse if necessary and identify by block number)					
<p>A detailed Monte Carlo simulation of the flow within an ion sampling mass spectrometer is described. The simulation includes effects of nonequilibrium flow and acceleration due to electric fields. A scheme for proton hydrate reactions is presented, including estimations of rate constants for agglomeration of H_2O onto positive ion clusters and lifetimes of the resulting complex. Complexes can be collisionally excited or stabilized within the model.</p> <p>Test calculations are performed for altitudes of 30 and 38 km. No significant effect of agglomeration of H_2O onto ion clusters was predicted in either case, but collisional excitation and subsequent dissociation of clusters was found to be a potentially severe problem.</p>					
20. DISTRIBUTION/AVAILABILITY OF ABSTRACT <input type="checkbox"/> UNCLASSIFIED/UNLIMITED <input checked="" type="checkbox"/> SAME AS RPT <input type="checkbox"/> DTIC USERS			21. ABSTRACT SECURITY CLASSIFICATION Unclassified		
22a. NAME OF RESPONSIBLE INDIVIDUAL Christopher Sherman			22b. TELEPHONE (Include Area Code)		22c. OFFICE SYMBOL AFGL/LID

ILLUSTRATIONS

1.	A Diagram of the Basic Solution Procedure Utilized in the EXPANDO Monte Carlo Transition Flow Code	3
2.	Schematic Showing the Major Features and Flow Regions Involved in the Expansion of a Gas Through a Sonic Orifice into a Near Vacuum	5
3.	The Discharge Coefficient for a Sharp Edged Orifice as Measured by Smetana, Sherrill and Schort	10
4.	A Drawing of a Cell Mesh of the Type Used in EXPANDO	13
5.	ADO Rate Constants for Cluster Formation as a Function of Cluster Size and Collision Velocity	34
6.	The Local Loss of $H^+(H_2O)_5$ Ion Clusters as a Function of Axial Position for the 30 Km Test Case	40
7.	The Integrated Effect of Agglomeration on Ion Clusters as a Function of Axial Position for the 30 Km Test Case	42
8.	The Integrated Effect of Agglomeration on Ion Clusters as a Function of Axial Position for the 38 Km Test Case	43
9.	The Integrated Effect of Fragmentation on Ion Clusters as a Function of Axial Position for the 30 Km Test Case	44
10.	The Integrated Effect of Fragmentation on Ion Clusters as a Function of Axial Position for the 38 Km Test Case	45
11.	The Axial Dependence of Ion Cluster Number Density for the 30 Km Test Case	46
12.	The Axial Dependence of Ion Cluster Number Density for the 38 Km Test Case	47
13.	The Total Calculated Effect of Fragmentation and Agglomeration on the $H^+(H_2O)_3$ Number Density as a Function of Axial Position for the Two Test Cases	48
14.	The Total Calculated Effect of Fragmentation and Agglomeration on the $H^+(H_2O)_4$ Number Density as a Function of Axial Position for the Two Test Cases	50

Illustrations (Continued)

15. The Total Calculated Effect of Fragmentation and Agglomeration on the $H^+(H_2O)_5$ Number Density as a Function of Axial Position for the Two Test Cases 51

TABLES

1.	Properties of the $N_2 + H_2O + H^+(H_2O)_n \rightleftharpoons N_2 + H^+(H_2O)_{n+1}$ Reactions	27
2.	Parameters for RRK Treatment of Cluster Dissociation	29
3.	Collision Rate, $v\sigma_L$, for $N_2 + [H^+(H_2O)_{n+1}]$	32
4.	Parameters Giving the Velocity Dependence of the Rate for the Process $H_2O + H^+(H_2O)_n \rightarrow [H^+(H_2O)_{n+1}]^*$	35
5.	Instrument Parameters Input to EXPANDO for the Sample Calculations	36
6.	Atmospheric Parameters Used in the Sample Calculations	37
7.	Air Molecular Parameters Used in the Sample Calculations	38

Accession For	
NTIS CRA&I	<input checked="" type="checkbox"/>
DTIC TAB	<input type="checkbox"/>
Unannounced	<input type="checkbox"/>
Justification	
By	
Distribution /	
Availability Codes	
Dist	Avail and/or Special
A-1	



1. INTRODUCTION

This is the final report of a three year effort to study physical processes of relevance to the mass spectrometric measurement of stratospheric ions. The effort involves the development of a Monte Carlo model of the free jet expansion occurring within the mass spectrometer including the effects of agglomeration onto, and fragmentation of, ionic clusters. This model has been named the EXPANDO code.

The attempt to carry out in situ mass spectrometry in the stratosphere is complicated by collision induced changes which may occur in the gas stream as it expands after passage through the orifice. Both positive and negative ions exist in the stratosphere with clustered polar molecules surrounding the ion core. As these ion clusters are carried along in the expanding gas stream, the falling temperature will tend to favor the formation of larger clusters. The charge-dipole interaction is characterized by large cross sections, so agglomeration of polar molecules can potentially alter the cluster size distribution that the quadrupole sees from the distribution that exists in the undisturbed stratosphere. Conversely, the measured cluster size distribution may be driven towards smaller clusters via fragmentation. As the ionic clusters are selectively accelerated by the electric field within the mass spectrometer, high energy collisions with neutrals may break apart the clusters.

The present effort involves a Monte Carlo simulation of these processes, so that a model can be used to relate the measured properties to those existing in the undisturbed atmosphere. The direct simulation Monte Carlo method involves storing a discrete number of molecules (via their velocities, positions and other pertinent information) in a computer. The solution region is broken up into a number of cells, and the solution is stepped forward in time in a two stage process. First, the molecules are advanced along their trajectories by an amount appropriate to their

velocity and a time increment Δt_m . In this first stage some molecules will leave the solution region and some will be introduced as determined by the boundary conditions. The second stage is to simulate collisions in each cell appropriate to Δt_m so that collision frequencies are properly simulated. A basic hypothesis of the method is that if the time step is made small enough the processes of translations and collisions can be uncoupled in this manner.

After a steady state has been achieved, the solution is periodically sampled by accumulating statistical sums of number densities, velocities and other basic properties. The solution is run repeatedly until statistical deviations are reduced to a desired limit, and then physically meaningful output quantities are computed from the statistical sums. The number of molecules represented is typically a few thousand at a time, which is vastly fewer than the number occurring in virtually all real flows. Hence, the construction of a dynamically similar flow to be simulated in the computer is an essential feature of the method.

The logic of the solution procedure for steady state flows is shown in Figure 1, which includes the steps described above. Section 2 is a discussion of the gas dynamics of a freejet expansion, and Section 3 presents the calculational grid developed for the EXPANDO code. The basic elements of the direct simulation Monte Carlo method have been described elsewhere,^{1,2} and they are presented here only briefly. The application of the technique to the mass spectrometer problem is discussed in Section 4, and the chemical scheme for proton hydrate reactions is developed in Section 5. Sample calculations and results are presented in Section 6.

¹Bird, G. A., Molecular Gas Dynamics, Clarendon Press, Oxford, 1976.

²Elgin, J. B., "Monte Carlo Calculations of Mass Spectrometer Flow", Report AFGL-TR-83-0057, Air Force Geophysics Laboratory, February 1983.

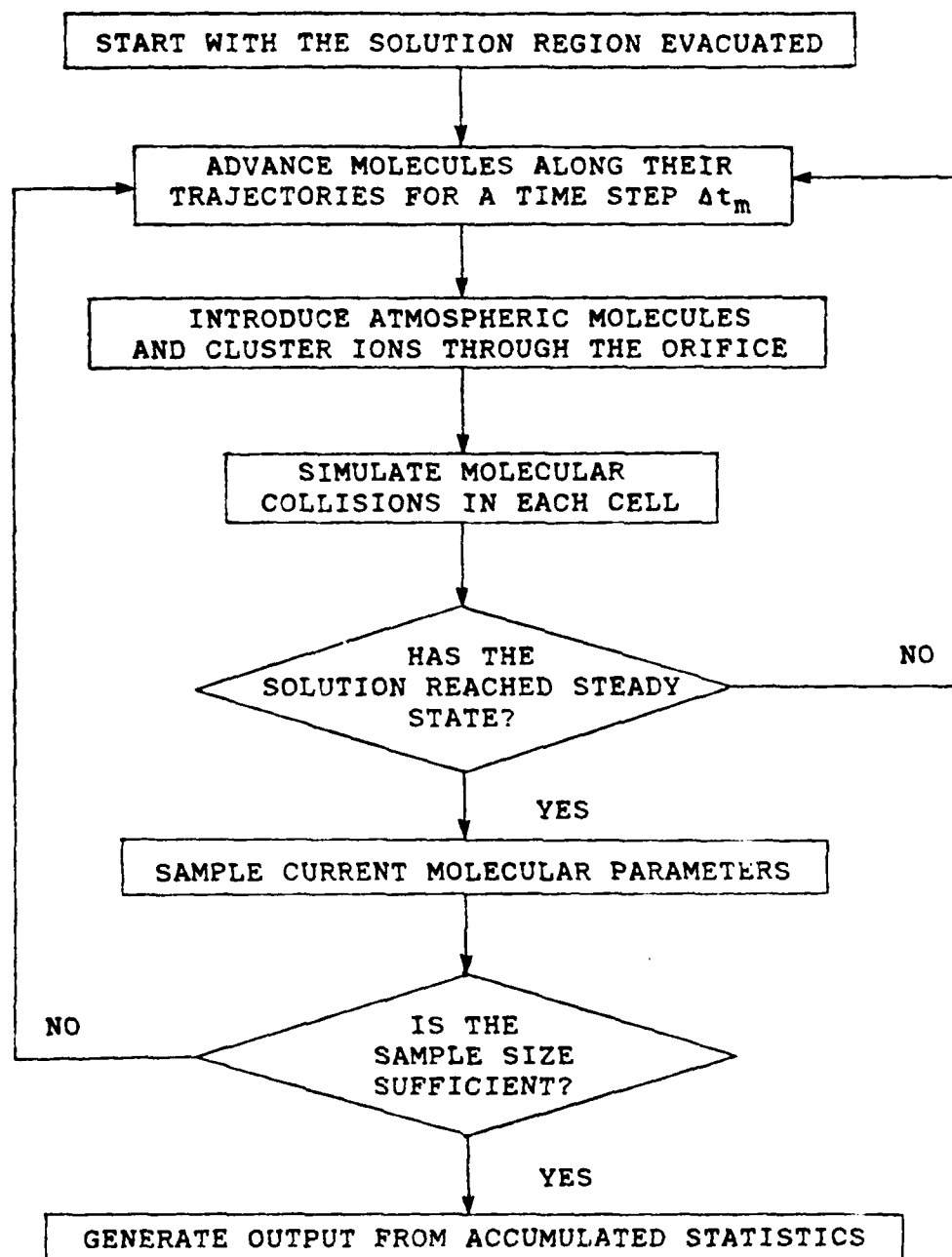


Figure 1. A Diagram of the Basic Solution Procedure Utilized in the EXPANDO Monte Carlo Transition Flow Code.

2. THE FREEJET EXPANSION WITHIN A MASS SPECTROMETER

2.1 Motivation for Studying Major Species Freejet

The freejet expansion of the major (neutral) species through a sonic orifice into a near vacuum is a classic problem representing the zeroth order solution to the problem at hand. The numerical dominance of the major species assures that their distribution in phase space (i.e., their density and velocity distributions) will be negligibly affected by the minor species of interest (e.g., ion clusters, H_2O , etc.). Hence, for a given atmospheric pressure and orifice geometry the freejet expansion of the major species can be calculated once and for all. The physical processes of interest (ion acceleration due to electric fields, agglomeration, fragmentation, etc.) are then handled by considering the minor species to be traveling within a known phase space distribution of major species. Considerable conceptual and computational simplifications result from the recognition that the freejet expansion is uncoupled from the ionic motion.

2.2 Physical Description of the Freejet Expansion

The major features of a freejet created by expanding air through a sonic orifice into a near vacuum are illustrated in Figure 2. For the cases of interest the orifice is always considerably larger than an ambient mean free path, so the initial portion of the expansion is best described in terms of continuum fluid mechanics. The orifice forms a sonic throat in which the flow is accelerated to a Mach number of unity. If the orifice has a finite thickness ("t" in Figure 2), then a boundary layer forms on the edge of the orifice, restricting the flow somewhat from that which would be predicted via one-dimensional inviscid theory. The mass flow through the orifice can be represented by³

SSI-82-024

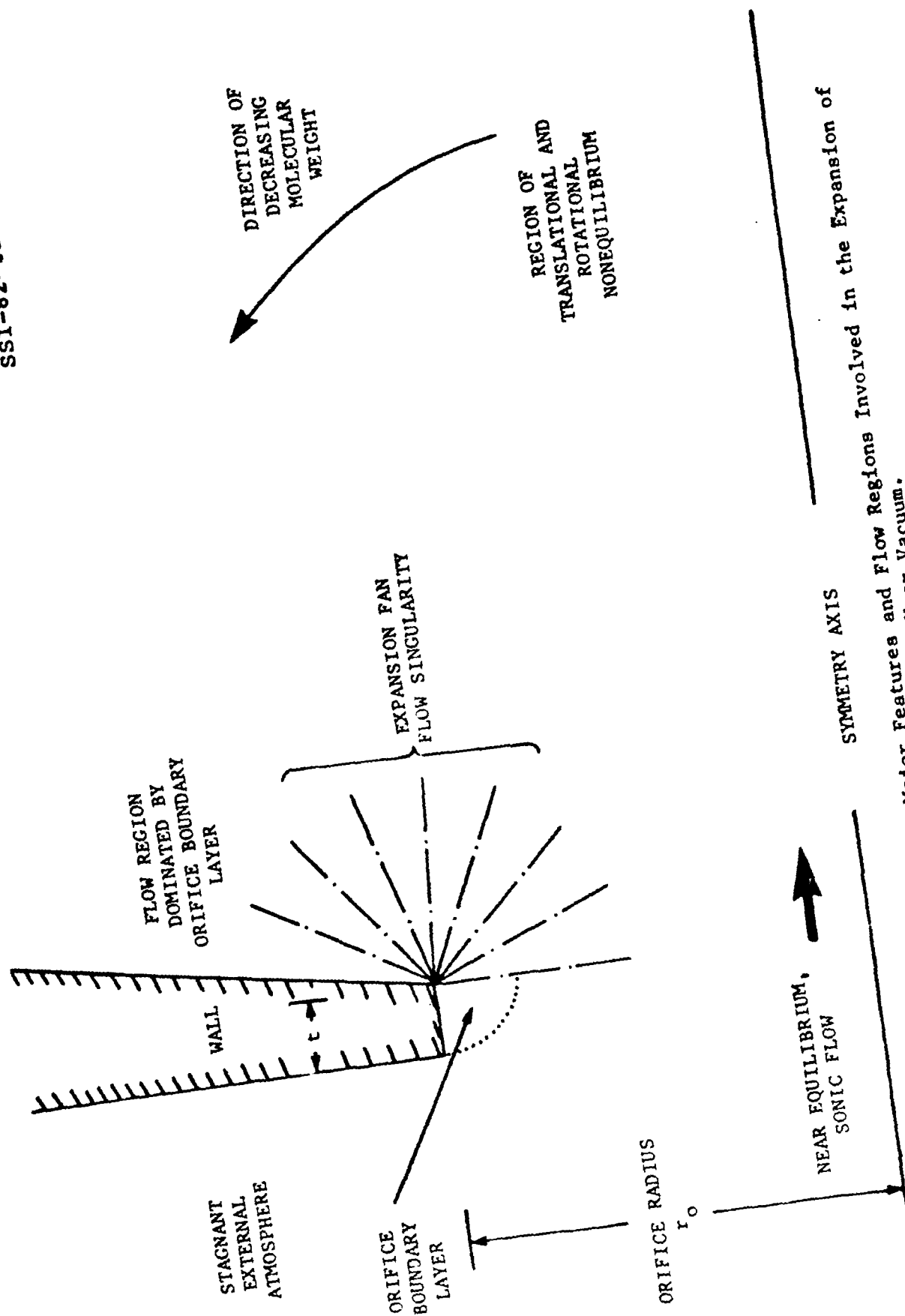


Figure 2. Schematic Showing the Major Features and Flow Regions Involved in the Expansion of a Gas Through a Sonic Orifice into a Near Vacuum.

$$\dot{m} = C_D (\pi r_0^2) \sqrt{\gamma P_0 \rho_0} [2/(\gamma + 1)]^{1/2} \{(\gamma + 1)/[2(\gamma - 1)]\}^{1/2} \quad (1)$$

where r_0 is the orifice radius, γ is the ratio of specific heats in the gas and P_0 and ρ_0 are the stagnation pressure and density, respectively. The discharge coefficient, C_D , is a corrective factor to bridge the gap between the ideal and real worlds. C_D is less than unity due to the presence of the orifice boundary layer (viscosity influence) and two dimensional flow effects.

As the gas passes through the orifice, an expansion fan is formed on the inner edge of the orifice and spreads out into the flow field. The expansion fan is initially describable in terms of Prandtl-Meyer theory, but is altered from that form as it proceeds away from the orifice by axisymmetric (as opposed to planar) flow effects.

The initial portion of the supersonic expansion is well suited for calculation via the method of characteristics (MOC),³ although the interaction of the boundary layer with the expansion fan is difficult to treat analytically. As the flow proceeds away from the orifice the rotational and randomized translational energy is transferred to directed kinetic energy of the flow. The flow expansion and consequent reduction in collision frequency, causes the gas to depart from thermal equilibrium. A residual rotational energy remains in the gas after collisions cease, and this is often characterized by a rotational temperature. (The populated rotational states do not, in general, adhere to a Boltzmann distribution;⁴ but this is of no great consequence to the present investigation.) Furthermore, the expansion is characterized by distinct parallel and

³Shapiro, A.H., The Dynamics and Thermodynamics of Compressible Fluid Flow, the Ronald Press Co., New York, 1953, pp. 73-105.

perpendicular temperatures representing residual randomized kinetic energy in directions parallel to and perpendicular to the mean flow direction.

The portion of the jet at large angles from the symmetry axis is dominated by the slower, more easily turned, gas from the orifice boundary layer. Also, the lighter molecular weight species become more concentrated at large angles from the symmetry axis leaving the central portion of the jet more concentrated in species with heavier molecular weights.⁵

2.3 Real Orifice Flow Effects

In principle, it would be possible to compute the flow from the undisturbed atmosphere into the mass spectrometer in a single solution. In such a solution, the boundary conditions applied would correspond to:

- 1) An undisturbed atmosphere bounding the appropriate portion of the solution region.
- 2) A wall interaction representing the molecular collisions with the mass spectrometer casing as well as the sides of the orifice.
- 3) Possible downstream conditions if the solution is carried to the point where interaction with the background gas within the mass spectrometer is important.

Although wall boundary conditions do have a degree of approximation that reflects our incomplete understanding of the gas-surface interaction

⁴Sharafudinov, R.G. and Skovorodko, P.A., "Rotational Level Population Kinetics in Nitrogen Freejets," Proceedings of the 12th International Symposium on Rarefied Gas Dynamics, AIAA Press, 1980.

⁵Bird, G.A., "Breakdown of Continuum Flow in Freejets and Rocket Plumes," Proceedings of the 12th International Symposium on Rarefied Gas Dynamics, AIAA Press, 1980.

process, the above boundary conditions are relatively well characterized. However, the above procedure does involve a substantial amount of computational effort aimed at the flow outside of the mass spectrometer, since that flow is usually characterized by a relatively small mean free path. Since the primary interest of the present study is to describe the flow within the mass spectrometer, it is natural to try to reduce the size of the solution region while retaining the essential portion of the flow. The obvious way to do this is to approximate the flow at the orifice, and merely compute the flow within the instrument.

There are several reasons to believe that such a procedure would be fruitful. If the orifice were a smooth walled converging-diverging nozzle, then the flow would expand to a Mach number of unity in the orifice plane, and it would be known exactly (except for boundary layer and two dimensional effects) irrespective of the flow downstream of the orifice. Although the actual orifice has a sharp edge, intuition implies that the downstream flow can have at best a small effect on the orifice flow, so it would seem plausible to specify the orifice flow a priori. Furthermore, the present study is concerned mainly with the flow along the centerline of the resulting jet, where boundary layer and two dimensional effects are minimized.

Although it would seem to be a classic problem, the expansion from a uniform state through a sharp edged orifice into a vacuum has apparently not been the object of intense study. Liepmann⁶ considered the problem in some detail, and indicated that the flow in the plane of the orifice is subsonic along the centerline, going supersonic and then back to sonic as the edge of the orifice is approached. Little else was said in this or any

⁶Liepmann, H.W., "Gaskinetics and Gasdynamics of Orifice Flow," Journal of Fluid Mechanics, Vol. 10, No. 5, 1961, pp. 65-79.

other available reference about the actual flow in the orifice plane. Measurements were presented, but they were limited to the discharge coefficient, which was subsequently measured by Smetana, Sherrill and Schort⁷ to greater accuracy. The results of the latter study are presented in Figure 3, which has been replotted to obtain a more convenient form. (As presented in Reference 7 both axes involved the unknown mass flow, so an iteration was required to determine the discharge coefficient. This problem is removed when the Reynold's number is defined in terms of available reference quantities rather than the unknown mass flow. The two Reynold's numbers differ only by a factor of the discharge coefficient.)

Use of the discharge coefficient presented in Figure 3 accounts for the major effect of a sharp edged orifice as opposed to a smooth nozzle, and it is apparently the only available effect for which measurements exist. The approach used in the EXPANDO code is to adjust the orifice mass flow to reflect the results of Figure 3, but the mean flow velocity is still assumed to start at sonic conditions. (Individual molecules, of course, will have a distribution of velocities about the mean.) Any error incurred via this procedure should have little effect on the centerline solution of interest.

2.4 Justification of Computational Approach

For the most part the departure of the freejet from local thermodynamic equilibrium marks the end of the region of validity for continuum techniques such as the method of characteristics. (An exception to this is a recent paper by Labowski, Ryali, and Fenn using the so-called

⁷Smetana, F.O., Sherrill, W.A., and Schort, D.R., "Measurements of the Discharge Characteristics of Sharp-edged and Round-edged Orifices in the Transition Regime," Proceedings of the 5'th Rarefied Gas Dynamics Symposium, Vol. 2, Academic Press, 1967.

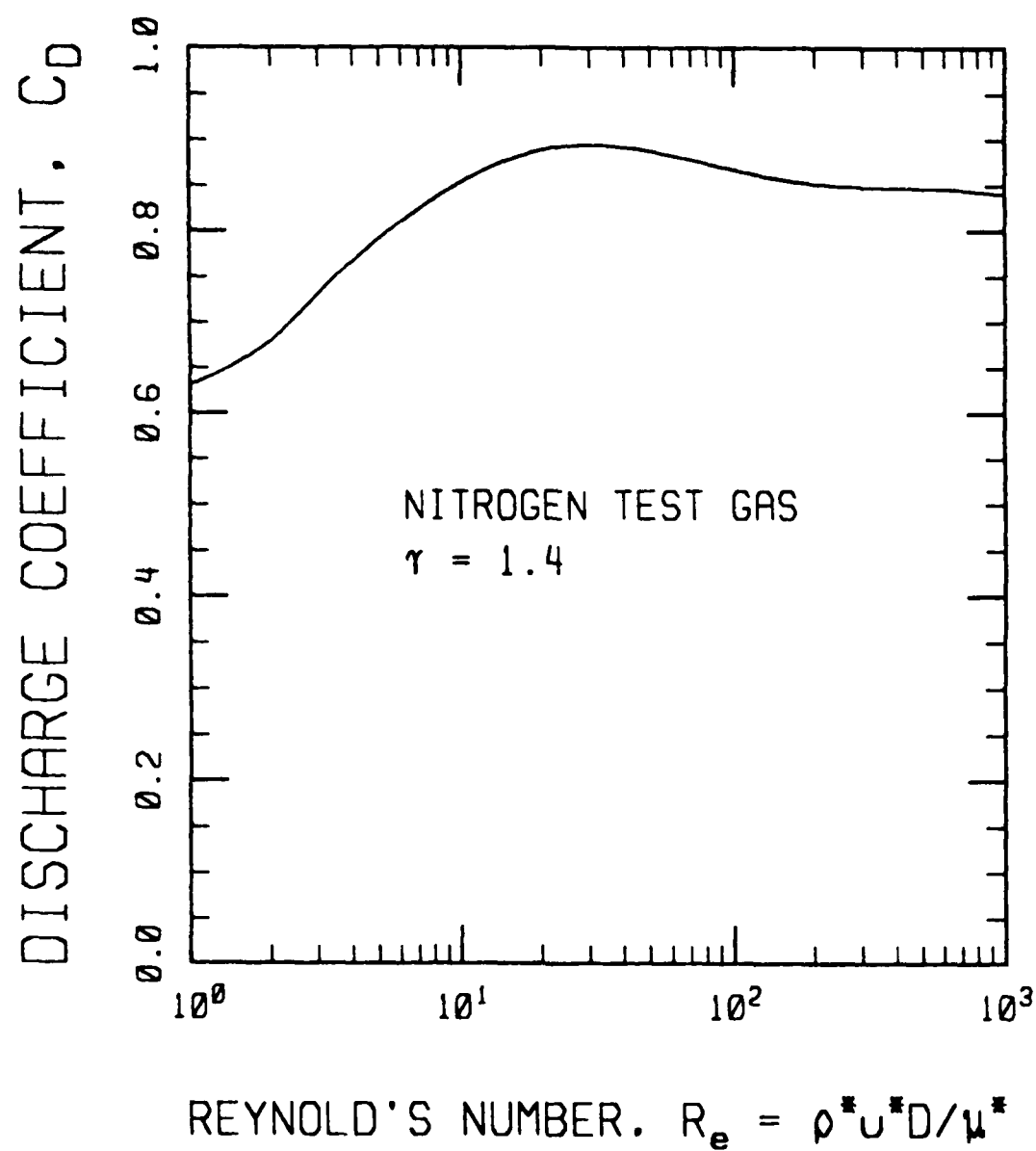


Figure 3. The Discharge Coefficient for a Sharp Edged Orifice as Measured by Smetana, Sherrill and Schort.⁷ It is plotted here as a function of Reynold's number based on sonic conditions and the orifice diameter.

nonequilibrium method of characteristics on a rotationally relaxing freejet.⁸ However, the method does not apply when the translational modes go out of equilibrium. Since the region between rotational and translational nonequilibrium is usually small, the method is inappropriate in the present study.)

The only presently available computational technique which is capable of describing the critical molecular processes occurring in the latter portions of the expansion is the direct simulation Monte Carlo Method. There was no choice to be made for the calculational technique to be used in the nonequilibrium portion of the expansion; the only question is whether the Monte Carlo method should have been used for the entire solution region, or whether it should have been wedded to a MOC calculation of the equilibrium portion. The answer to this question depended largely on how large the equilibrium region was expected to be. (It should be stressed that the Monte Carlo flow field is valid for equilibrium continuum flow -- but it is less efficient computationally.) The breakdown of translational and rotational equilibrium has been considered in some detail by Bird,^{5,9} and based on this work the conclusion is that a MOC calculation could not be used beyond two orifice radii from the orifice at an altitude of 20 km and essentially could not be used at all at 40 km altitude. This very limited range of validity for a MOC calculation indicated that the preferred calculational approach was simply to use a Monte Carlo method for the entire flow field.

⁸Labowski, M. Ryali, S., and Fenn, J.B., "Flowfield Calculations in Nonequilibrium Freejets by the Method of Characteristics," Proceedings of the 12th International Symposium on Rarefied Gas Dynamics, AIAA Press, 1980.

⁹Bird, G.A., "Breakdown of Translational and Rotational Equilibrium in Gaseous Expansions," AIAA Journal, Vol. 8, No. 11, November 1970, pp. 1997-2003.

3. CALCULATIONAL GRID

3.1 General Considerations

The selection of grid geometries for fluid mechanic calculations can generally be regarded as more of an art than a science. Considerations in the selection of a grid are:

- * The grid should be as simple as possible, since the program must repeatedly decide what cell molecules are in as they move. If this required the solution of a complex equation, the entire program would run significantly slower than if the cell can be determined easily.
- * The grid should concentrate cells where gradients are the largest, so that the least number of total cells (and molecules) are needed to obtain an accurate solution.
- * The grid should provide output where it is required, with the resolution that is desired for the answer of interest.

The EXPANDO cell structure is illustrated schematically in Figure 4, and is characterized by the following relations:

- * The orifice radius is divided up evenly into a specified number of grid spacings. This number can be varied to achieve convergence.
- * Above the orifice, at the first axial location, there are some additional cells of the same size to help describe the expansion that occurs around the orifice edge. The number of cells above the orifice can also be varied to achieve convergence along the flow centerline (the region of importance for the present investigation).
- * The cells are constructed between a series of planes which are perpendicular to the jet axis. The spacing between successive planes increases as they proceed further from the orifice.

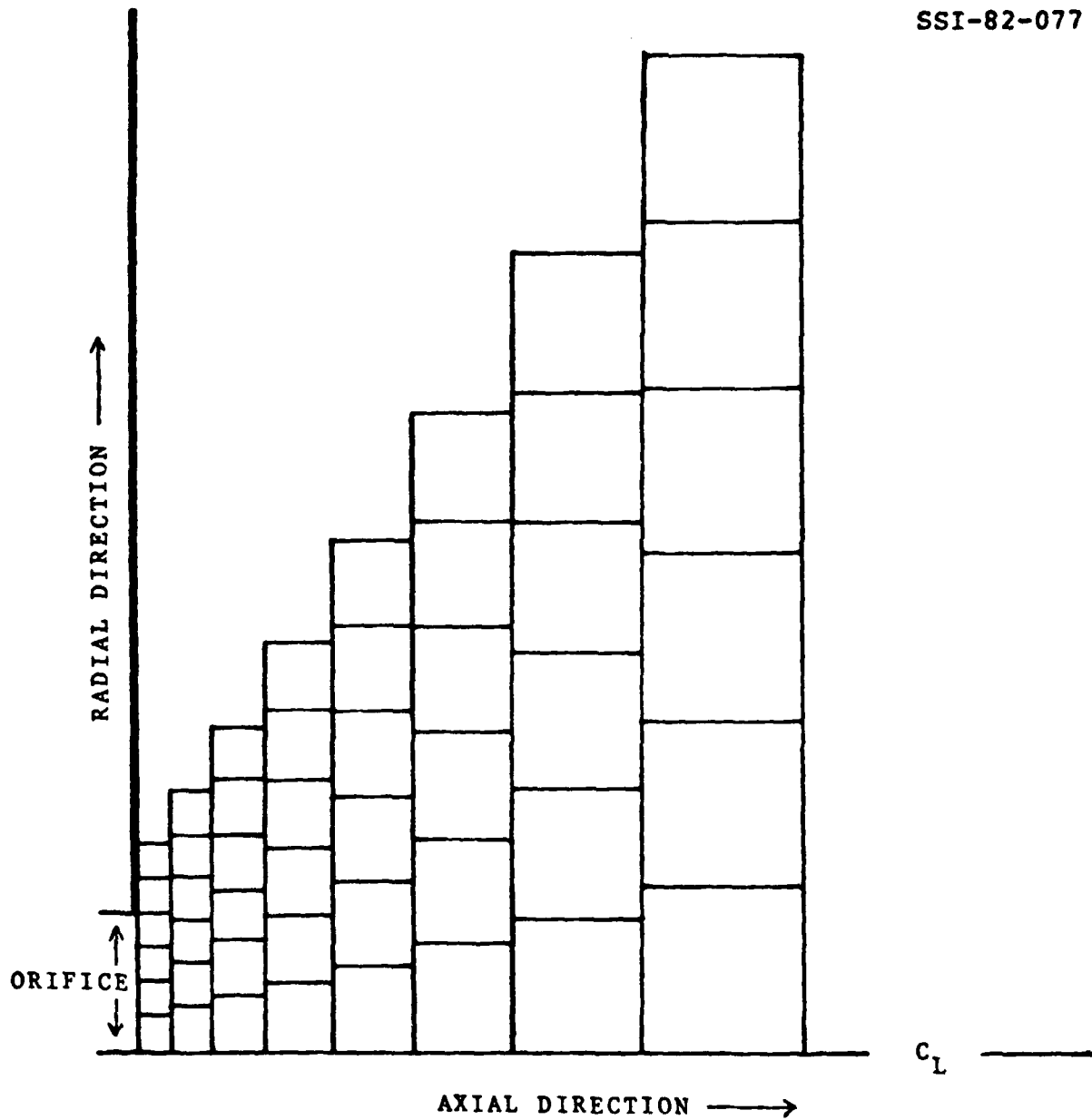


Figure 4. A Drawing of a Cell Mesh of the Type Used in Expando.

since the flow gradients will decrease in this direction. The rule for the increase of the spacing between the planes is given by the equation:

$$\frac{\Delta Z_j}{r_0 + Z_j} = A = \text{constant} \quad , \quad (2)$$

where Z_j is the location of the J 'th plane and ΔZ_j is the spacing between it and the previous plane (i.e., $\Delta Z_j = Z_j - Z_{j-1}$), and r_0 is the orifice radius. This relation can be solved to give the location of Z_j directly as:

$$Z_j = r_0 [(1-A)^{-j} - 1] \quad . \quad (3)$$

This relation is easily inverted to find the axial cell location of a particular molecule.

- * The cells are selected to have a radial increment equal to the axial increment, and the number of cells per axial location is kept constant. Hence, as the cells grow larger in the axial direction, they automatically keep pace in the radial direction.

3.2 Spatial Segmentation Of The Solution Region

The code was written so that it has the ability to compute sequential spatial segments of the solution starting from the orifice. (This ability is merely an option and in no way affects the capability of handling the entire flow field at once.) The use of this option offers the potential for a substantial decrease in the memory and computing time required to solve a problem. Details of the spatial segmentation scheme are discussed in the subsections below.

3.2.1 Justification for Segmentation

The first question that must be addressed is whether the segmentation of the solution is physically and mathematically justified, and this

question is critically related to the question of boundary conditions. The physical laws that are embodied in the Monte Carlo solution procedure, involving molecular translations and collisions, are as valid for a portion of the solution region as they are for the whole region. In order to carry out the solution in just a subregion, however, it is necessary that the boundary conditions can be specified a priori along the boundaries of the subregion in question.

For a Monte Carlo flow field calculation, the boundary conditions are imposed by specifying the velocity distribution function for incoming molecules along all boundaries, and then selecting molecules from this distribution with the proper frequency and introducing them into the simulation. Usually this involves extending the boundaries to a region of undisturbed (known) flow, or to a region where molecular backflow into the solution region is insignificant.

In the simulation of mass spectrometer flow, the upstream boundary is taken to correspond to one dimensional sonic conditions at the orifice, except that the mass flow is reduced by an empirically determined discharge coefficient. The solution region is extended far enough downstream and to the side so that the flow of molecules into the solution region from these other boundaries can be neglected. (An exception to this is the incursion of background gas into the jet which could be treated as an equilibrium gas at the side boundaries. This feature is not included in the code nor does it affect the present discussion since the distribution function for this gas would be assumed known at the side boundaries.) Hence, a well defined solution can be carried out downstream of the orifice as long as the downstream boundary is far enough from the orifice to assure that molecular backflow is negligible. Since molecules have a thermal velocity which is on the order of the speed of sound, backflow becomes negligible when the local Mach number is large compared to unity. (It is interesting to contrast this to a continuum calculation, which requires only that the

local Mach number be greater than one, perhaps by a very small amount, for there to be no upstream influence.) In a Maxwellian gas, the probability of an individual molecule having an upstream velocity direction is given by P , where

$$P = \frac{1}{2} \text{erfc}(M\sqrt{\gamma/2}) \quad , \quad (4)$$

and M and γ denote Mach number and ratio of specific heats, respectively. For sonic flow this probability is on the order of 5%, but by the time the Mach number has become 2.0 the probability is on the order of 4×10^{-4} and, for all practical purposes, backflow can be ignored.

Hence, the imposition of the downstream boundary condition neglecting backflow into the solution region is justified very shortly after the orifice, since the flow rapidly becomes substantially supersonic. As long as this is the case, it is perfectly proper to solve for a small segment of the solution region. Once that solution is completed, then the derived velocity distribution on the downstream boundary defines the required upstream boundary condition for the next solution segment. This information is automatically written to a file which is, in turn, automatically read as input for the next segment.

3.2.2 Advantages of Segmentation

Although the physical justification for segmenting the solution region has been demonstrated, there remains the question as to why one would want to "turn one problem into two or more problems". Frequently the subdivision of a physical problem into multiple subproblems reduces the total effort involved, and this is no exception. Specific advantages are enumerated below.

3.2.2.1 Reduced Storage

When the problem is broken up into segments, the total number of cells and molecules required in any one segment is less than required for the larger single solution. This translates directly into a decreased requirement for computer core.

3.2.2.2 Decreased Time to Achieve Steady Flow

The Monte Carlo technique is inherently a procedure which solves an unsteady flow problem. For cases such as the present one where the problem of interest is really a steady state flow, this is solved by letting the unsteady solution relax to a steady state. The computation time required to achieve a steady state can be regarded as "computational overhead" for the present problem, since useful steady state sampling of the solution cannot begin until steady state has been achieved.

The time required to establish a steady flow can be estimated a priori as the length of the solution region divided by the orifice flow velocity (times a safety factor). Hence, the longer the initial solution segment, the greater is the period of unsteady flow. If the entire solution region is calculated at once, then the program may well spend most of its effort in simply achieving steady state. If the solution region is segmented, however, then the first segment can reach steady state substantially faster than the whole solution region does. This is of particular significance since the solution near the orifice is the most collision dominated, requiring a large portion of the computational effort needed in each time step. When subsequent segments are solved, they still require a relatively long time to achieve steady state (though the time is somewhat diminished since the solution region is shorter), but the computational effort per time step is substantially less.

3.2.2.3 Increased Time Step for Latter Segments

The time step in a Monte Carlo simulation should generally be small compared to the mean time between collisions for a molecule, since the processes of translation and collisions are treated separately in each time step. If the entire solution is solved for at once, this implies that the entire solution is constrained to the relatively small time step required by the collisional region near the orifice. If that region is solved for separately, then subsequent segments can have a substantially larger time step since the mean time between collisions is larger in subsequent segments. Hence, even though the latter regions still require a relatively large amount of simulation time to achieve steady state, this time is more easily accomplished since the allowable time step is much larger.

3.2.3 Segmentation Summary

These considerations strongly suggest that the first spatial segment should be made within a few diameters of the orifice, since: 1) The flow is by then already sufficiently supersonic to justify the neglect of backflowing molecules, and 2) The number of time steps required to achieve steady state is small, which is particularly important in this collision dominated region of the flow. Note that the question is completely unrelated to whether or not the flow is in equilibrium (as would be the case if an initial region were to be calculated by the method of characteristics). It is simply a matter of making the calculation of the flow field more efficient by separating the relatively long relaxation time which is required by the latter portions of the flow field from the collision dominance which is characteristic of the initial portion. Once the first segment is calculated, then subsequent segments benefit computationally from the ability to take substantially larger time steps in those regions.

4. GAS MODEL

The details of the Monte Carlo solution procedure are described extensively in References 1 and 2; a summary of the major features of the method is provided here for completeness. Unlike early Monte Carlo models, the molecules are allowed to possess internal energy, and interact with velocity dependent cross sections.

4.1 Collision Cross Sections

The available translational collisional energy between the two molecules, E_c , is given in terms of their relative velocity, c_r , by

$$E_c = \frac{1}{2} \mu_{ij} c_r^2 \quad (5)$$

where μ_{ij} is the reduced mass of the pair; i.e.

$$\mu_{ij} = \frac{m_i m_j}{m_i + m_j} \quad (6)$$

and m_i and m_j represent the molecular masses. The code utilizes the Variable-Hard-Sphere (VHS) model,¹⁰ where molecules have a collision cross section which varies as an inverse power of the available collision energy. Hence, if σ_{ij} is the collision cross section for collisions of species i with species j , then σ_{ij} is given by a relation of the form

¹⁰Bird, G. A., "Monte-Carlo Simulation in an Engineering Context", Proceedings of the 12th International Symposium on Rarefied Gas Dynamics, Vol. 74, Progress in Astronautics and Aeronautics, AIAA, New York, 1981.

$$\sigma_{ij} = A_{ij} E_c^{-\omega} \quad , \quad (7)$$

where A_{ij} is a constant coefficient.

The parameter ω can be related to η , the exponent of distance in an inverse power intermolecular force law via the relation¹⁰

$$\omega = \frac{2}{\eta-1} \quad . \quad (8)$$

Hence, hard sphere molecules (for which η goes to infinity) are represented by ω equal to zero. There is a substantial body of evidence, however, that the effective size of molecules does indeed decrease with increasing collision energy, so a positive value of ω is usually a better choice. ω can be determined from molecular beam data, or from its macroscopic implications. For example, if s is the exponent for the variation of the viscosity coefficient with temperature, then it can be shown¹⁰ that

$$s = \omega + 0.5 \quad , \quad (9)$$

so a measurement of the temperature dependence of the viscosity coefficient serves as an indirect determination of ω . It was on this basis that a value of ω equal to approximately 0.24 is recommended for the major species (air) flow.

Although the sizes of molecules are allowed to vary in the VHS model in deciding whether or not a collision is to occur, when a collision does occur the post collision velocity components are computed as if it were a hard sphere collision. This results in a substantial computational simplification and yet retains good agreement with the macroscopic predictions of the more exact model.¹⁰

4.2 Weighting Factors

Statistical weighting factors are a crucial element of a successful Monte Carlo simulation, allowing trace species to be described with reasonable accuracy. The weighting factor is the number of "real" molecules that correspond to each "simulated" molecule. A "simulated" molecule corresponds to one molecule's worth of storage allocated in the program, and the weighting factor is its statistical weight. The weighting factors used in EXPANDO are dependent on cell and species. The weighting factors are dynamically adjusted as the simulation proceeds, keeping the number of simulated molecules more or less constant while allowing the number of real molecules to adjust as the solution evolves.

4.3 Collision Mechanics

4.3.1 Elastic Collisions

Conservation of momentum implies that the center-of-mass velocity of a collision pair is unchanged by the collision; and conservation of energy then implies that the magnitude of the relative velocity between the collision partners is also unchanged by the collision.¹¹ Since the collision is treated as a statistical event, all that remains is to select the direction of the post collision relative velocity vector from the correct distribution. As mentioned earlier, collisions in the VHS model are treated as hard sphere collisions when they occur (though they do not occur with the same velocity dependence as do hard sphere collisions). For such molecules, all directions for the post collision relative velocity

¹¹Vincenti, Walter G., and Kruger, Charles H., Jr., Introduction to Physical Gas Dynamics, John Wiley and Sons, 1965, pp. 348-356.

vector are equally likely. This is the chief computational simplicity of the VHS model. An elastic collision is simulated by selecting a new direction for the relative velocity vector and then computing the corresponding molecular velocities.

4.3.2 Inelastic Collisions

Molecules are allowed to have internal energy which is described via the phenomenological model of Borgnakke and Larsen.¹² In this model, transfer of energy between internal and translational modes is allowed, but it is necessary to assume that each species has a fixed number of internal degrees of freedom, ζ_i . A collision is assumed to be either perfectly elastic or perfectly inelastic via a user specified probability. A perfectly inelastic collision is achieved by summing the total pre-collision energy (i.e., the internal energy of both molecules plus the translational energy of their relative motion) and then assigning post collision values from the equilibrium distribution for collisions with that total amount of energy, taking into account the number of internal degrees of freedom in the two molecules. Note that this model has the ability to relax from a nonequilibrium to an equilibrium state via an effective collision number. The ability to exchange internal energy in such a manner comprises a significant increase in capability for Monte Carlo codes beyond the previous models where molecules had no internal energy. It is this capability which enables the codes to realistically predict the macroscopic effects of polyatomic gas flow. This model predicts an overall level of internal (usually rotational) energy, but it does not describe individual

¹²Borgnakke, Claus, and Larsen, Paul S., "Statistical Collision Model for Monte Carlo Simulation of Polyatomic Gas Mixture", Journal of Computational Physics, Vol. 18, 1975, pp. 405-420.

quantum states. When this is desired, it can be accomplished by considering the separate states to be distinct species.

Let ζ_1 and ζ_2 be the number of internal degrees of freedom of the two molecules in an inelastic collision, and E_s be the total collision energy defined by

$$E_s = E_{ci} + E_{1i} + E_{2i} \quad , \quad (10)$$

where E_{ci} is the initial translational collision energy defined by Eq. (5), and E_{1i} and E_{2i} are the pre-collision internal energies of the two molecules. The somewhat cumbersome expressions given in Ref. 12, can be recast in terms of the Chi-Square distribution. Post-collision values for the respective energies are given by

$$E_{1f} = \frac{X_1 E_s}{X_1 + X_2 + X_3} \quad , \quad (11)$$

$$E_{2f} = \frac{X_2 E_s}{X_1 + X_2 + X_3} \quad , \quad (12)$$

and

$$E_{cf} = \frac{X_3 E_s}{X_1 + X_2 + X_3} \quad , \quad (13)$$

where X_1 is selected from a Chi-Square distribution with ζ_1 degrees of freedom, X_2 is selected from a Chi-Square distribution with ζ_2 degrees of freedom and X_3 is selected from a Chi-Square distribution with $2(2-\omega)$ degrees of freedom. The post collision translational energy is then used to determine a new relative velocity between the two molecules.

4.3.3 Reactive Collisions

Reactive collisions can be simulated directly in the EXPANDO code. The treatment of reactive collisions is similar to that for inelastic collisions, except that a heat of reaction is added to the total energy expressed in Eq. (10). The reaction is simulated with a probability which is proportional to the ratio of the reactive to collision cross section at the relative velocity for the collision. Reactive collisions can result in the disappearance of reactant molecules, with the post collision state being applied to the product molecules.

5. KINETICS OF PROTON HYDRATE REACTIONS

Laboratory and in situ mass spectrometer measurements¹³ indicate that stratospheric positive ions undergo significant dissociation in the presence of electric fields of moderate strengths ($0 \rightarrow 20$ V/cm). In order to understand this type of phenomena, we have investigated the kinetics of the proton hydrate (PH) reactions. The PH system was chosen for two reasons: (1) in situ measurements of low hydration order PH show abundances much greater than theoretical (thermodynamic) predictions and (2) there are numerous experimental results on the kinetics and thermodynamics of PH reactions. In the remainder of this section, we discuss the experimental results pertinent to the PH reactions, as well as the approximate theories for the agglomeration/fragmentation processes, which are used in the Monte Carlo simulation.

¹³Arnold, F., Henschen, G., and Ferguson, E. E., "Mass Spectrometric Measurements of Fractional Ion Abundances in the Stratosphere-Positive Ions," *Planet. Space Sci.* 29(1981), pp. 185-193.

5.1 Laboratory Measurements of PH Reactions

The overall reaction in which we are interested is



where $n=1,2,\dots,5$ and M represents the third body. Usually, such ion agglomeration/fragmentation reactions are represented by the following mechanism:



and



[For notational simplicity, the cluster size index, n , has been suppressed in writing the rate constants. It should be apparent to the reader that k_f , k_r , etc. refer to the appropriate rate constant for a particular cluster size, i.e., $k_{f,n}$, $k_{r,n+1}$, etc.]. Assuming steady state for $[\text{H}^+(\text{H}_2\text{O})_{n+1}]^*$ allows the overall forward and reverse rates to be written in terms of the individual rates for Eqs. (15)-(18) as

$$k_f = \frac{k_c k_s [\text{M}]}{k_d + k_s [\text{M}]} \quad (19)$$

and

$$k_r = \frac{k_a k_d [M]}{k_d + k_s [M]} \quad (20)$$

In the low pressure limit (i.e., $k_d \gg k_s [M]$), Eqs. (19) and (20) reduce to

$$k_f = \frac{k_c k_s}{k_d} [M] = k_f^0 [M] \quad (21)$$

and

$$k_r = k_a [M] = k_r^0 [M] \quad (22)$$

There have been extensive experimental studies to determine the rate constants, k_f^0 , as a function of PH cluster size with $M=N_2$,¹⁴ O_2 ,¹⁵ and CH_4 .¹⁶ For $M=CH_4$, the temperature dependence of k_f^0 was also determined over a wide temperature range for $n=1,2,\dots,5$. The latest (and probably most accurate) measurements of the equilibrium constant ($K=k_f/k_r$) are those of Kebarle et al.¹⁶ It is important to note that there are no direct measurements of the reverse rate, k_r^0 . However, values of k_r^0 have been

¹⁴Good, A., Durden, D. A., and Kebarle, P., "Ion Molecule Reactions in Pure Nitrogen and Nitrogen Containing Traces of Water at Total Pressures 0.5-4 torr. Kinetics of Clustering Reactions Forming $H^+(H_2O)_n$," J. Chem. Phys. 52(1970), pp. 212-221.

¹⁵Good, A., Durden, D. A., and Kebarle, P., "Mechanism and Rate Constants of Ion-Molecule Reactions Leading to Formation of $H^+(H_2O)_n$ in Moist Oxygen and Air," J. Chem. Phys. 52(1970), pp. 222-229.

¹⁶Lau, Y. K., Ikuta, S., and Kebarle, P., "Thermodynamics and Kinetics of the Gas-Phase Reactions: $H_3O^+(H_2O)_{n-1} + H_2O \rightleftharpoons H_3O^+(H_2O)_n$," J. Am. Chem. Soc. 104(1982), pp. 1463-1469.

obtained using the forward rates and equilibrium constants. The experimental data which are most relevant to the present work are summarized in Table 1.

Table 1. Properties of the $N_2+H_2O+H^+(H_2O)_n \rightleftharpoons N_2+H^+(H_2O)_{n+1}$ Reactions.

n	$K_{n,n+1}^a$ (cm^3)	$k_{f,n}$ (cm^6/sec)	$k_{r,n+1}$ (cm^3/sec)	$-\Delta H_{n,n+1}^a$ (kcal/mole)	b^d
1	2.060×10^{-2}	3.4×10^{-27b}	1.7×10^{-25}	31.6	4
2	1.207×10^{-10}	2.3×10^{-27b}	1.9×10^{-17}	19.5	7.5
3	3.405×10^{-10}	2.4×10^{-27b}	7.0×10^{-15}	17.9	8.1
4	4.909×10^{-16}	1.5×10^{-27c}	3.1×10^{-12}	12.7	14
5	3.966×10^{-17}	---	---	11.6	15.3

^aFrom ref. 16

^bFrom ref. 14

^cFrom ref. 15 Adjusted to 300 K and $M=N_2$.

^dFrom ref. 16 The parameter b gives the temperature dependence of $k_{f,n}$, i.e., $k_{f,n} \sim T^{-b}$.

The data given in Table 1 will provide the necessary checks and (sometimes) inputs for the theoretical cross sections which will be developed in the following sections.

5.2 Rate of $[H^+(H_2O)_{n+1}]^*$ Decomposition

The rate of unimolecular decomposition (Eq. (17)) can be estimated from classical RRK theory.¹⁷ It has recently been shown¹⁸ that a classical

RRK description of Ar clustering provides a semi-quantitative description of the unimolecular decomposition. The form of the (1st order) rate constant is

$$k_d = A((E-E_0)/E)^{s-1} \quad , \quad (23)$$

where the constant A is the limiting rate, E is the total energy of the complex, E_0 is the critical energy for dissociation, and s is the effective number of oscillators in the complex. In the present case, A is chosen arbitrarily (albeit judiciously), E_0 is the thermodynamic dissociation energy, and s is approximately equal to b+1, where b is the temperature dependence of the measured forward rate (see Table 1). The total energy of the complex is given by

$$E = \frac{1}{2}\mu v^2 + E_0 + sRT \quad , \quad (24)$$

where we have assumed the internal energy of the complex is sRT. Table 2 contains the parameters appropriate to the PH complexes. It is interesting to note that the values of s deduced from experiment correlates very nicely with 3N-6 (3N-5 for a linear complex), if one assumes that the H₂O ligands have no internal degrees of freedom.

¹⁷See, for example, Forst, W., Theory of Unimolecular Reactions (Academic Press, N. Y., 1973).

¹⁸Brady, J. W., Doll, J. D., and Thompson, D. L., J. Chem. Phys. 73(1980), pp. 2767-2772.

Table 2. Parameters for RRK Treatment of Cluster Dissociation.

n	A (sec ⁻¹)	E ₀ (ergs/molec)	s exp.	s theory
1	2x10 ¹³	2.1955x10 ⁻¹²	5	4
2	1x10 ¹⁴	1.3548x10 ⁻¹²	8	6
3	1x10 ¹⁴	1.2437x10 ⁻¹²	9	9
4	1x10 ¹⁴	8.8237x10 ⁻¹³	15	12
5	1x10 ¹⁴	8.0595x10 ⁻¹³	16	15

5.3 Theoretical Cross Sections for PH Reactions

The cross sections for the above processes can usually be obtained in analytical form using simplified theories of ion-molecule collisions.^{19,20} In general, rate constants for ion-molecule reactions display either no temperature dependence or a negative temperature dependence. Since

¹⁹Castleman, A. W., "Nucleation and Molecular Clustering About Ions," Advances in Colloid and Interface Science 10(1979), pp. 73-128, and references therein.

²⁰Hsieh, E. T. -Y. and Castleman, A. W., "A Reconsideration of the Theory of Capture Cross Sections for Ion/Molecule Reactions and a Total Energy and Angular Momentum Conserved Average Charge-Dipole Interaction Theory," International Journal of Mass Spectrometry and Ion Physics 40(1981), pp. 295-329.

ion-molecule cross sections are usually controlled by long range forces, collisions not only lack an activation energy, but they also possess large cross sections. The first semi-quantitative treatment of ion-molecule collisions involved the use of the Langevin expression for an ion-induced dipole long range interaction. Interestingly, the rate constant calculated using the Langevin approach shows no temperature dependence. Since the Langevin expression shows the essential features of the collision theories appropriate for the present study, we will consider this approach in detail. The extension of the Langevin-type treatment of collision dynamics should then be obvious.

The basic idea in the Langevin approach is that the collision cross section is completely determined by long range interactions, allowing an extremely complicated N-body scattering problem to be reduced to a simple two-body problem. The total energy for the two-body problem is given by

$$\frac{1}{2}\mu v^2 = T_R + V_{\text{eff}} \quad , \quad (25)$$

where μ is the reduced mass between the collision partners, v is the initial relative velocity, T_R is the relative translational energy. V_{eff} is the effective potential energy given by

$$V_{\text{eff}} = \frac{(\mu v b)^2}{2\mu R^2} - \frac{\alpha e^2}{2R^4} \quad , \quad (26)$$

where b is the impact parameter, α is the polarizability of the neutral molecule, and e is the electronic charge. The effective potential, V_{eff} , defined by Eq. (26), possesses a maximum value for a particular value of $R=R_C$, which can be obtained from

$$\frac{dV_{\text{eff}}(v, b, R)}{dR} = 0 \quad (27)$$

For collisions with a relative translational energy, T_R , satisfying

$$T_R > \mu v^2 - V_{\text{eff}}(v, b, R_C) \quad (28)$$

the two particles have enough energy to surmount the centrifugal barrier ($=V_{\text{eff}}(v, b, R_C)$) and enter the strong collision region. If Eq. (28) is not satisfied, then the particles will be reflected and no chemical interaction can occur. In Langevin theory, it is assumed that once the particles enter the strong collision region, the reaction occurs with unit probability. The centrifugal barrier height depends on both v and b . For a specified v , the barrier height will increase with b , until an impact parameter is reached such that

$$\mu v^2 = V_{\text{eff}}(v, b_C, R_C) \quad (29)$$

Notice that in Eq. (29), the value of T_R is taken to be zero. From the above discussion, the only collisions leading to reaction are those with $b < b_C$. Therefore, the cross section for ion-molecule reactions is given by

$$\sigma_C = \pi b_C^2 \quad (30)$$

The value of b_C can be obtained from Eqs. (26), (27), and (29) as

$$b_C^2 = \frac{1}{v} \sqrt{4\alpha e^2 / \mu} \quad (31)$$

Notice that the expression for the Langevin cross section possesses an inverse velocity dependence, which results in a rate constant independent of temperature. This behavior is easily subsumed within the Monte Carlo formalism by choosing $\omega = 0.5$ in Eq. (7).

5.4 Complex Activation and Stabilization in the Monte Carlo Model

The ion-neutral collision cross section, σ_L , is obtained from Langevin theory. There is no ambient temperature dependence, only a dependence on the polarizability of the neutral molecule and the reduced mass of the collision partners. The collision rates are given in Table 3 for $M=N_2$.

Table 3. Collision Rate, $v\sigma_L$, for $N_2+[H^+(H_2O)_{n+1}]$.

n	$v\sigma_L$ (cm^3/sec)
1	7.7158×10^{-10}
2	7.1514×10^{-10}
3	6.8474×10^{-10}
4	6.6570×10^{-10}
5	6.5265×10^{-10}

Within the Monte Carlo framework, cluster ions are treated as "big molecules" with 2s internal degrees of freedom. There is no inherent difference in the treatment of activated and stable clusters other than the possession of internal energy greater than the dissociation energy. When a cluster is activated, it is assigned a lifetime from an exponential distribution with the mean value determined by Eq. (23). Every time a cluster (activated or not) undergoes a collision, it is treated as an inelastic collision (see Section 4.3.2), and a new internal energy and lifetime result. Hence, a cluster can be activated or stabilized in a collision depending upon the post-collision internal energy of the cluster ion. When it's lifetime comes up, a water molecule is dissociated off and the dissociation energy is removed from the product pair.

5.5 Cross Section for Complex Formation

The cross section for complex formation (see Eq. (15)), σ_c , can be obtained from the average dipole orientation (ADO) theory.²¹ The ADO theory is an extension of Langevin theory which allows the neutral molecule (i.e., H_2O) to possess a permanent, as well as induced, dipole moment. In this case, the effective potential is given by

$$V_{eff} = \frac{(\mu vb)^2}{2\mu R^2} - \frac{\alpha e^2}{2R^4} - \frac{\mu_d e}{R^2} \langle \cos \theta(R) \rangle \quad (32)$$

where μ_d is the dipole moment and $\theta(R)$ is the dipole orientation angle. The last term in Eq. (32) represents the orientation averaged charge-dipole interaction. Following the same procedure outlined above, we obtain for R_c and b_c

$$v^2 = \frac{\alpha e^2}{\mu R_c^4} + \frac{\mu_d e}{\mu R_c} \frac{d\langle \cos \theta \rangle}{dR} \quad (33)$$

and

$$b_c^2 = R_c^2 + \frac{\alpha e^2}{\mu v^2 R_c^2} + \frac{2\mu_d e}{\mu v^2} \langle \cos \theta \rangle \quad (34)$$

Eqs. (33) and (34) are implicit relations for R_c and b_c , which must be solved numerically. The cross sections are then obtained via Eq. (30).

The velocity dependent capture rate constants $v\sigma_c$ for $H_2O + (H^+H_2O)_n$ ($n=1,2,\dots,5$) are shown in Fig. 5, assuming an ambient temperature of 227 K. The (slight) ambient temperature dependence is due to the dipole rotation. At velocities near room temperature, the rate constant is nearly

²¹Su, T. and Bowers, M. T., J. Chem. Phys. **58**(1973), pp. 3027-3037. See Ref. 20 for criticism and corrections concerning this approach.

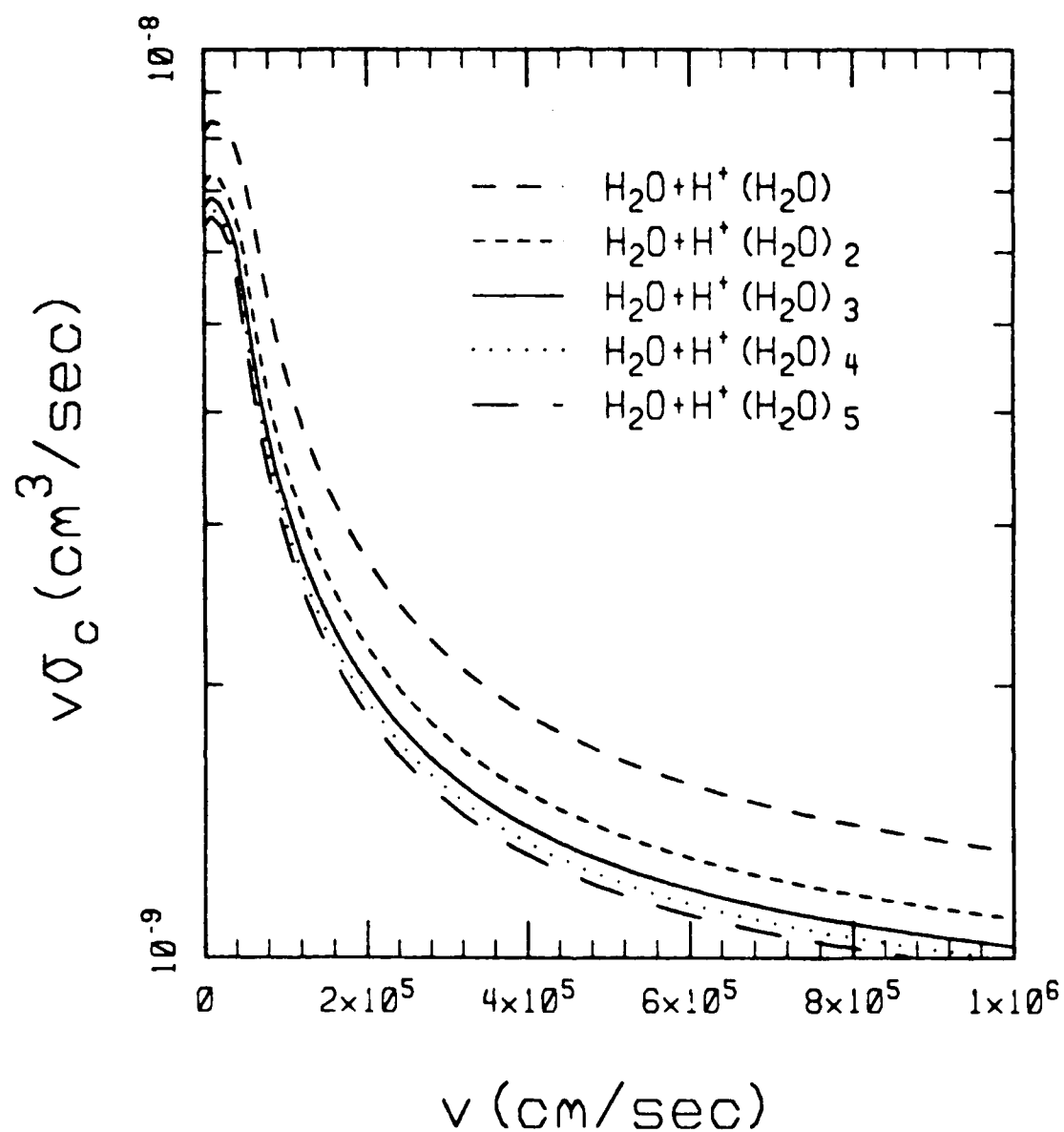


Figure 5. ADO Rate Constants for Cluster Formation as A Function of Cluster Size and Collision Velocity.

temperature independent. As the collision velocity increases, the capture rate decreases as $1/v$ until the Langevin (high velocity) limit is reached. Notice that ADO theory predicts a rate constant up to an order of magnitude greater than the corresponding Langevin rate. the capture rate constant decreases as the cluster size increases, due to the increase in the reduced mass of the collision partners.

As mentioned above, the result is not in closed form. Therefore, the calculated cross sections are fit to the following expression:

$$v\sigma_c = a_n \quad (v < v_n^*) \quad (35)$$

and

$$v\sigma_c = \frac{b_n}{v} + c_n \quad (v > v_n^*) \quad (36)$$

The parameters resulting from the fit of Eqs. (35) and (36) to the rates shown in Fig. 5 are given in Table 4.

Table 4. Parameters Giving the Velocity Dependence of the Rate for the Process $H_2O + H^+(H_2O)_n \rightarrow [H^+(H_2O)_{n+1}]^*$.

n	v_n^* (cm/sec)	a_n (cm ³ /sec)	b_n (cm ⁴ /sec ²)	c_n (cm ³ /sec)
1	4.9×10^4	8.316×10^{-9}	3.616×10^{-4}	9.372×10^{-10}
2	4.3×10^4	7.261×10^{-9}	2.770×10^{-4}	8.188×10^{-10}
3	4.1×10^4	6.791×10^{-9}	2.468×10^{-4}	7.721×10^{-10}
4	4.0×10^4	6.572×10^{-9}	2.329×10^{-4}	7.500×10^{-10}
5	3.9×10^4	6.476×10^{-9}	2.239×10^{-4}	7.350×10^{-10}

6. SAMPLE CASES WITH DISCUSSION

The EXPANDO code was exercised for two cases to produce quantitative results. These cases correspond to a single instrument operated at altitudes of 30 and 38 kilometers, and were designed to represent actual experimental cases as closely as possible. These cases are described in detail in the subsections below.

6.1 Instrument Parameters

The instrument was characterized in the code by the parameters given in Table 5. These are the only parameters of the instrument which are used by the EXPANDO code, and they are felt to be the important ones in determining the character of the initial, collision dominated, portion of the expansion which is of primary concern to the code.

Table 5. Instrument Parameters Input to EXPANDO for the Sample Calculations.

Parameter	Value	Units
Orifice Diameter	0.0406	cm
Orifice to Skimmer Distance	2.54	cm
Skimmer Diameter	0.9728	cm
Orifice Potential	-1.0	volt
Skimmer Potential	-50.0	volt

6.2 Atmospheric Parameters

The 1976 standard atmosphere was used to obtain the pressure and temperature at the two altitudes, and the water concentration was obtained

from Ref. 22. These inputs were then used in a model given in Ref. 23 to predict initial ion cluster concentrations to use in starting the calculation at the orifice.²⁴ These parameters are summarized in Table 6.

Table 6. Atmospheric Parameters Used in the Sample Calculations.

Parameter	30 Km Value	38 Km Value
Ambient Number Density (cm^{-3})	3.830×10^{17}	1.116×10^{17}
Ambient Temperature (K)	226.5	244.8
$\text{H}^+(\text{H}_2\text{O})_3$ Mole Fraction	3.43×10^{-18}	1.19×10^{-17}
$\text{H}^+(\text{H}_2\text{O})_4$ Mole Fraction	1.81×10^{-15}	6.20×10^{-15}
$\text{H}^+(\text{H}_2\text{O})_5$ Mole Fraction	3.27×10^{-15}	1.12×10^{-14}
$\text{H}^+(\text{H}_2\text{O})_6$ Mole Fraction	1.41×10^{-16}	4.84×10^{-16}
N_2 Mole Fraction	0.7885	0.7885
O_2 Mole Fraction	0.2115	0.2115
H_2O Mole Fraction	4.0×10^{-6}	5.5×10^{-6}

The velocity dependence of the cross sections for N_2 , O_2 and H_2O were determined from gas viscosity data,²⁵ using relations given in Ref. 10, and the number of internal degrees of freedom was determined from their ratio

²²Deguchi, S. and Muhleman, D. O., "Mesospheric Water Vapor", Journal of Geophysical Research, 87(C2), Feb. 20, 1982, pp. 1343-1346.

²³Kebarle, P., Annual Review of Physical Chemistry, 28, 1977, p. 445.

²⁴Ballanthin, J., Private Communication.

²⁵Handbook of Chemistry and Physics, 55th Edition, CRC Press, pp. F58.

of specific heats. (The ratio of specific heats was taken at 150 K, where the rotational modes of air are not fully excited. This led to less than two internal degrees of freedom for N_2 and O_2 .) A weighted mean value of $\omega=0.2428$ was used in the major species solution, and the reference values in Table 7 then define the variable A_{ij} in Eq. (7). The probability of a collision being elastic was taken to be 50%, except for collisions involving cluster ions which were always taken to be inelastic. A complete listing of the cluster ion parameters which were used was presented in Section 5.

Table 7. Air Molecular Parameters Used in the Sample Calculations.

Molecule	Reference Cross Section (cm^2)	Reference Velocity (cm/s)	Energy Exponent, ω	Internal Degrees of Freedom, ζ
N_2	5.902×10^{-15}	5.619×10^4	0.2277	1.444
O_2	6.101×10^{-15}	5.149×10^4	0.2992	1.640
H_2O	1.628×10^{-14}	6.182×10^4	0.6211	3.000

6.3 Calculational Results

The probability of a molecule undergoing a reaction per unit distance traveled is given by P , where

$$P = \dot{n}_r / (nv_z) \quad , \quad (37)$$

and \dot{n}_r is the volumetric reaction rate (reactions per unit volume per unit time), n is the local number density of reactant (molecules per unit

volume), and v_z is the local axial velocity. P gives a direct measure of the importance of a process as a function of position within the mass spectrometer. This parameter is shown in Figure 6 for the fragmentation (unimolecular decomposition) and agglomeration processes acting on $H^+(H_2O)_5$ at 30 km altitude. The minor wiggles in the curves are a result of statistical scatter in the Monte Carlo solution and have no physical significance. This scatter does not interfere with the interpretation of the curves.

The fragmentation process does not start until approximately 0.2 centimeters from the orifice, but it then rises rapidly and dies off relatively slowly downstream. This behavior is readily understood in terms of the relevant physics. Firstly, the unimolecular decomposition of clusters is primarily a result of collisional excitation of the clusters. Hence, it depends mainly on collision frequency and collision energy. These quantities are both considerably different for ion-neutral collisions than they are for neutral-neutral collisions. As the flow expands, the number densities decrease substantially. The relative velocity between neutrals drops considerably due to the decreasing temperature, but the relative velocity between ions and neutrals increases due to acceleration of the ions by the electric field. The result is that the collision frequency does not decrease nearly as rapidly for ion-neutral collisions as for neutral-neutral collisions. Similarly, when collisions occur, they occur at higher energies. All these factors combine to produce the relatively gentle slope in the fragmentation rate curve.

The agglomeration process is most important at the orifice, and decreases downstream to very small levels. Although agglomeration is also an ion-neutral process, it has a cross section which decreases with increasing energy (see Fig. 5), so it has a somewhat greater slope in the downstream region. However, the primary issue for agglomeration is that it involves the interaction of a cluster with a minor species (H_2O), which has

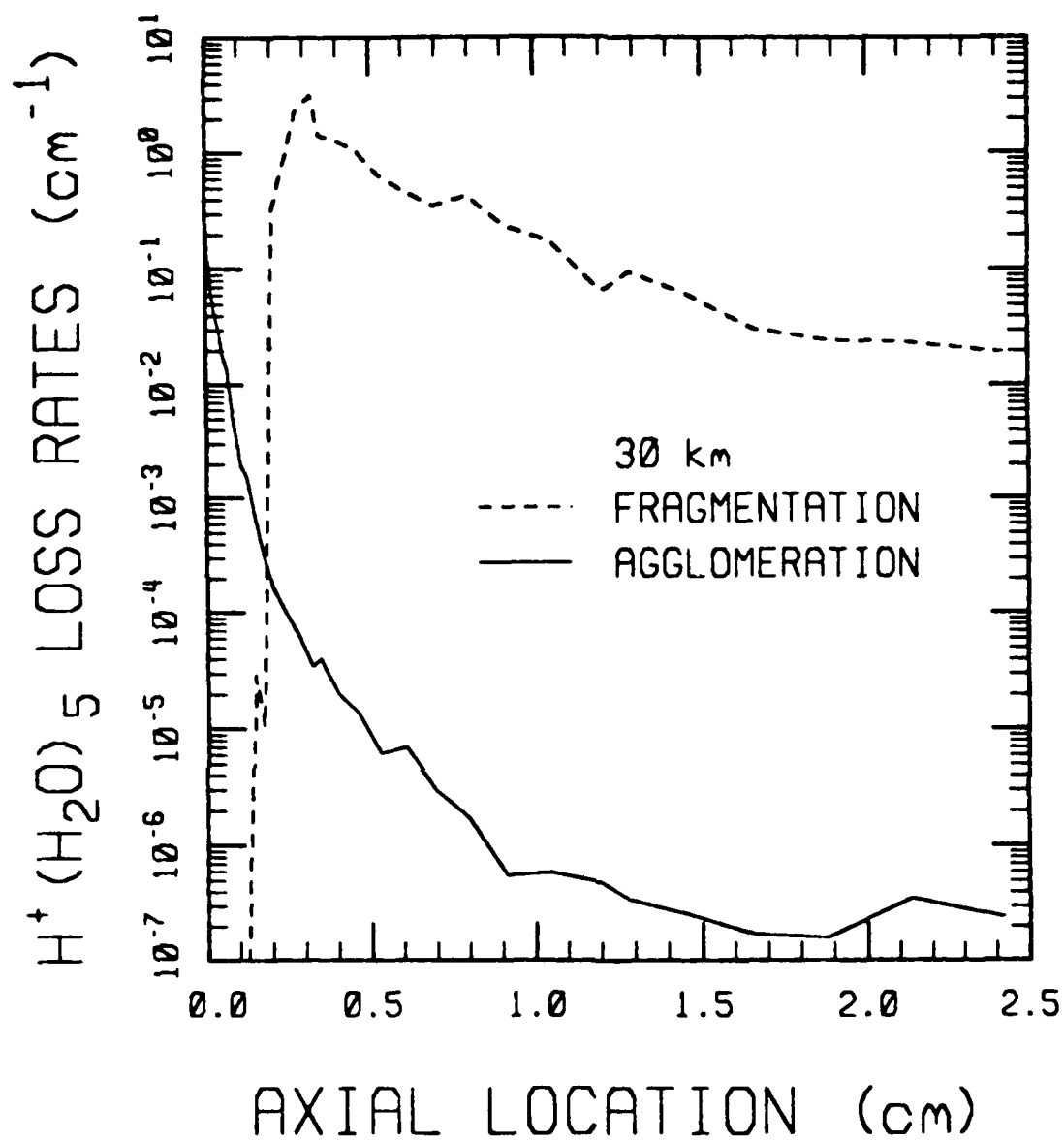


Figure 6. The Local Loss of $H^+(H_2O)_5$ Ion Clusters as a Function of Axial Position for the 30 Km Test Case.

a concentration of only a few parts per million. There are not enough collisions between the clusters and water for agglomeration to be a significant process in these calculations. This conclusion is made quantitatively in Figs. 7 and 8 for the 30 and 38 km cases. In these figures, the integrated probability of a cluster acquiring another water molecule is presented as a function of axial distance. At 30 km the probability is always less than 1%, and at 38 km its maximum is about $1\frac{1}{2}\%$.

Figures 9 and 10 show the integrated loss from fragmentation for the two altitudes. In contrast to the case for agglomeration, it can be seen that the probability of a cluster being fragmented in the mass spectrometer is on the order of 50% for 30 km and 25% for 38 km. The value is less for the higher altitude case due to the fewer collisions that occur at lower density, but the perturbation of the measured values would have to be considered significant at either altitude.

Figures 7-10 showed the loss rate for a particular type of cluster, without considering gain from any source. In a measurement, of course, the interpretation of the results is complicated by the fact that when a cluster fragments it produces another cluster with one less water molecule. The calculated ion cluster number densities are plotted as a function of axial position in Figures 11 and 12 for the two altitudes. The most obvious feature of these calculations is the abrupt increase in the number density of $H^+(H_2O)_3$ clusters in the region between 0.2 and 0.4 centimeters from the orifice. This feature is a result of fragmenting of $H^+(H_2O)_4$ clusters which are initially much more numerous than the $H^+(H_2O)_3$ clusters. For the $H^+(H_2O)_3$ clusters, fragmentation is not a 50% effect, it is an effect predicted to produce an increase of over two orders of magnitude. This is shown quantitatively in Fig. 13, which shows the integrated effect of both fragmentation and agglomeration on $H^+(H_2O)_3$, taking into account the increase brought on by the fragmenting of $H^+(H_2O)_4$ clusters. (It should be noted that the $H^+(H_2O)_3$ clusters were not allowed to fragment in the

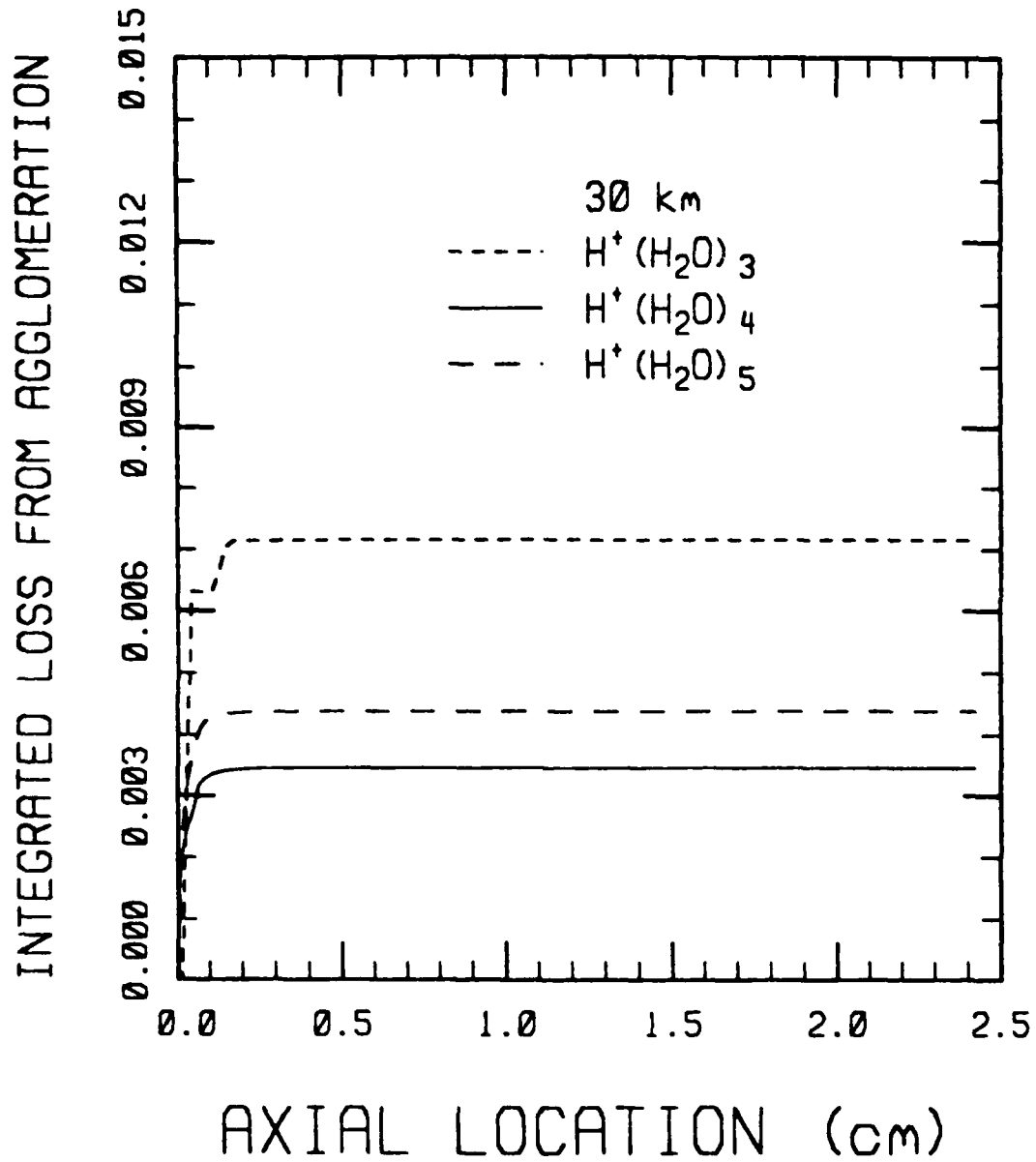


Figure 7. The Integrated Effect of Agglomeration on Ion Clusters as a Function of Axial Position for the 30 Km Test Case.

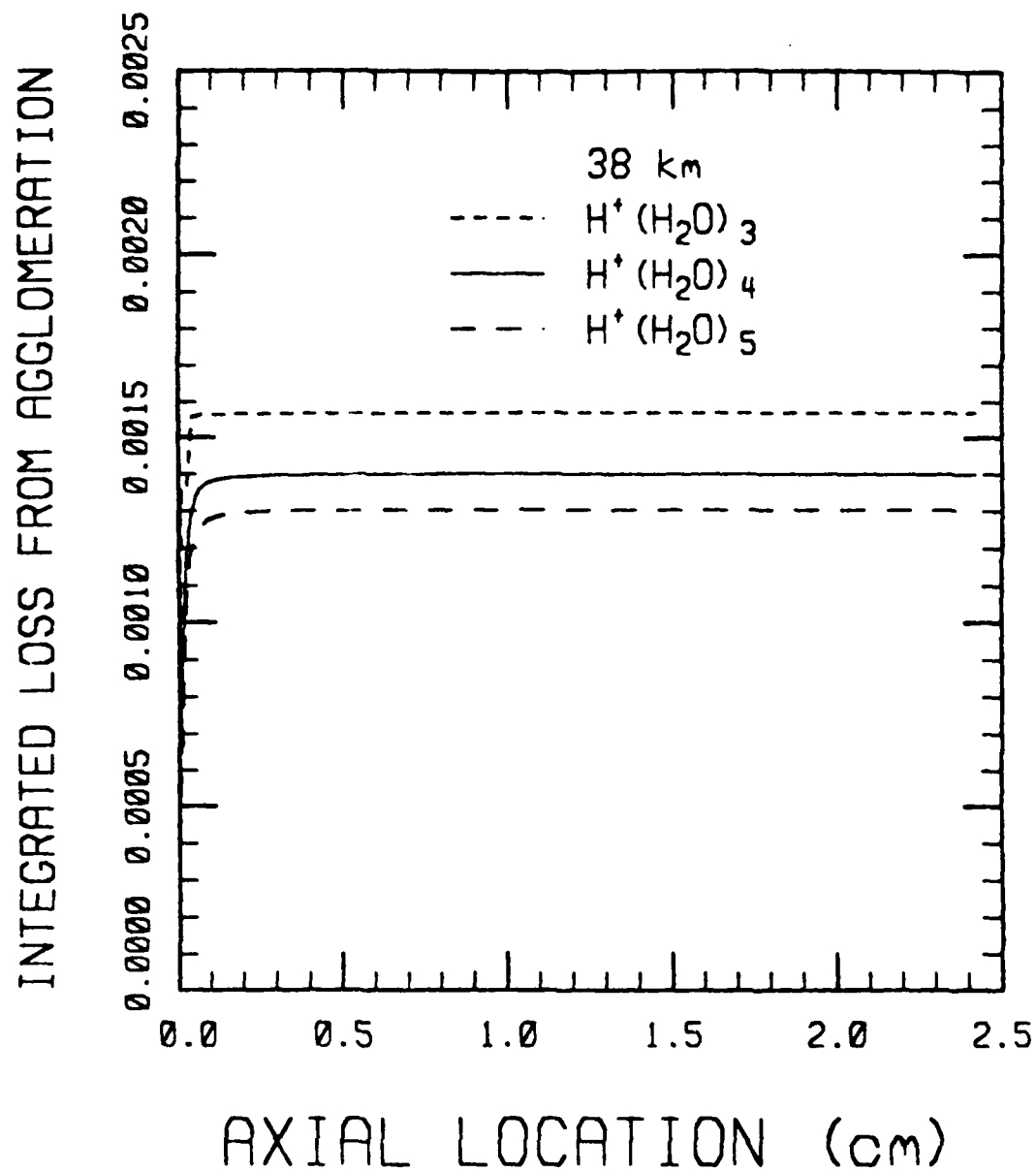


Figure 8. The Integrated Effect of Agglomeration on Ion Clusters as a Function of Axial Position for the 38 Km Test Case.

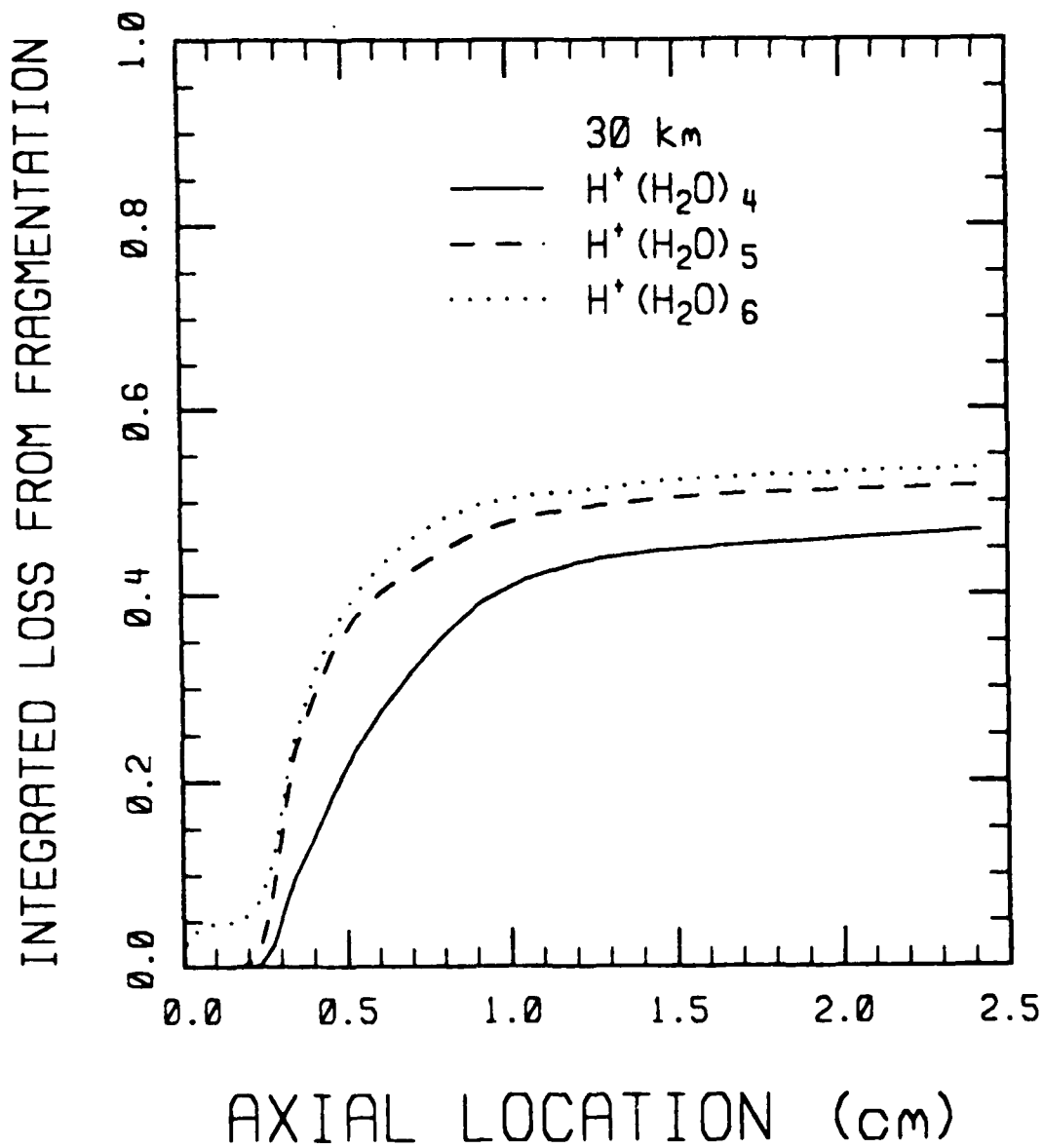


Figure 9. The Integrated Effect of Fragmentation on Ion Clusters as a Function of Axial Position for the 30 Km Test Case.

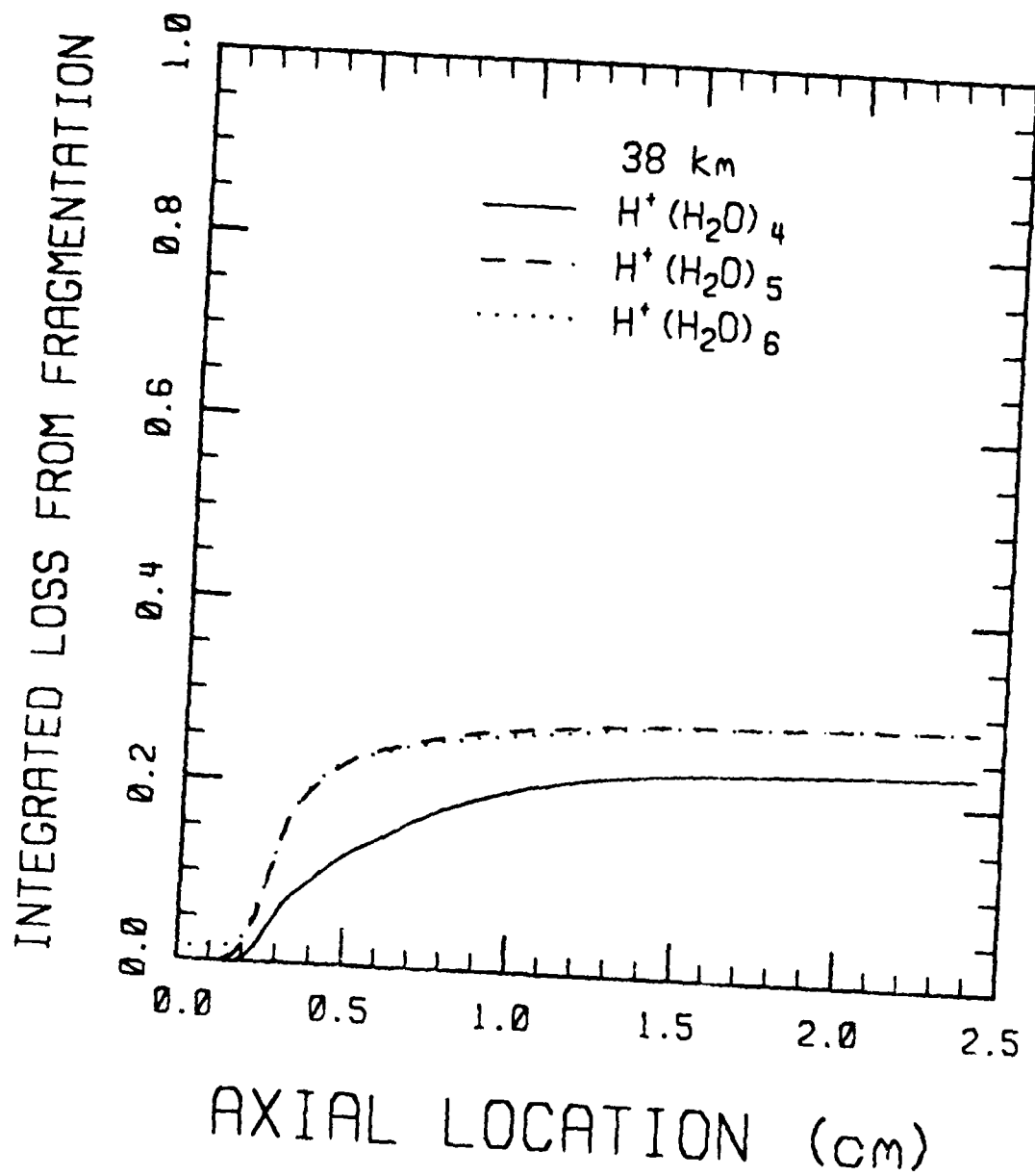


Figure 10. The Integrated Effect of Fragmentation on Ion Clusters as a Function of Axial Position for the 38 Km Test Case.

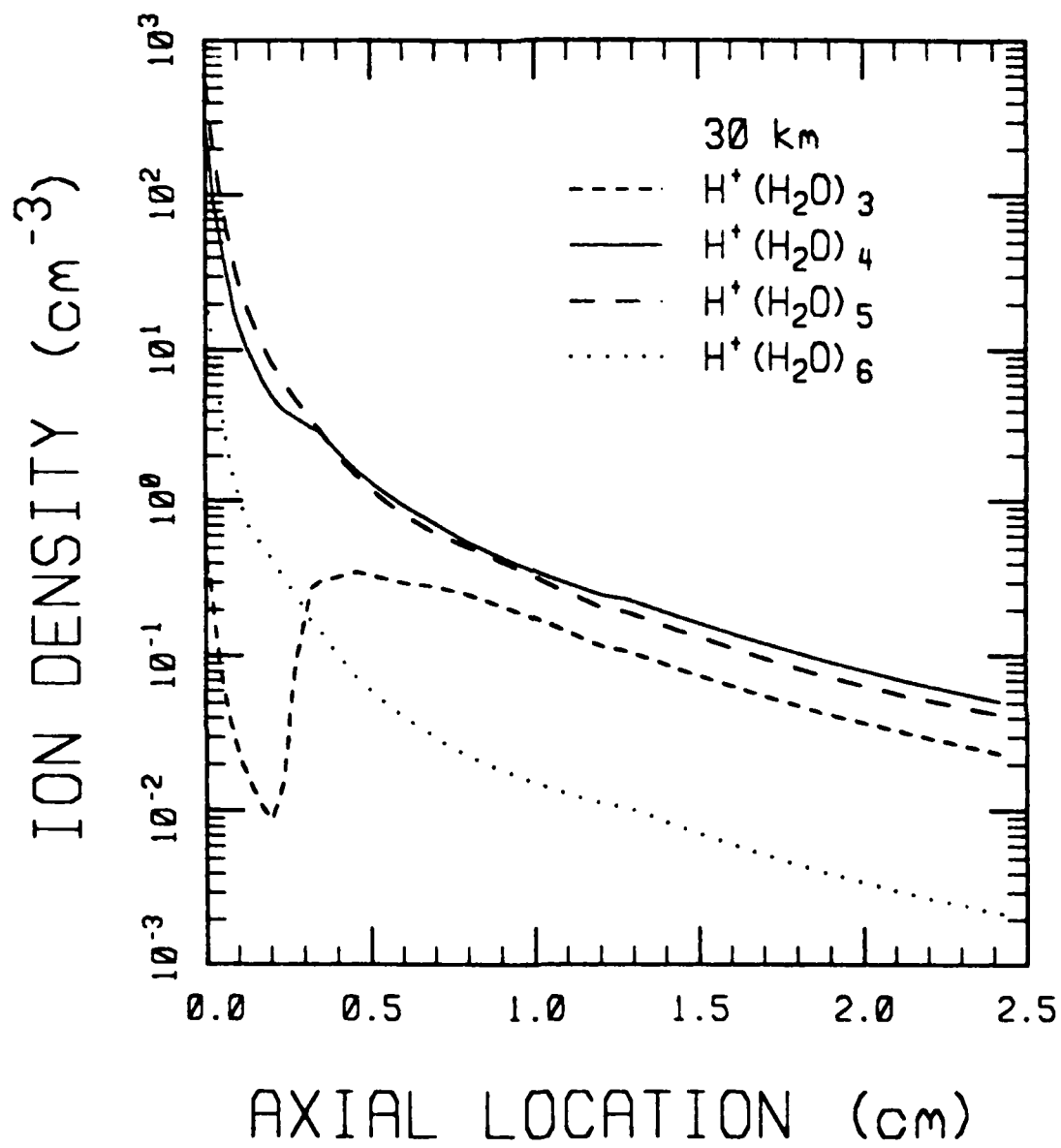


Figure 11. The Axial Dependence of Ion Cluster Number Density for the 30 Km Test Case.

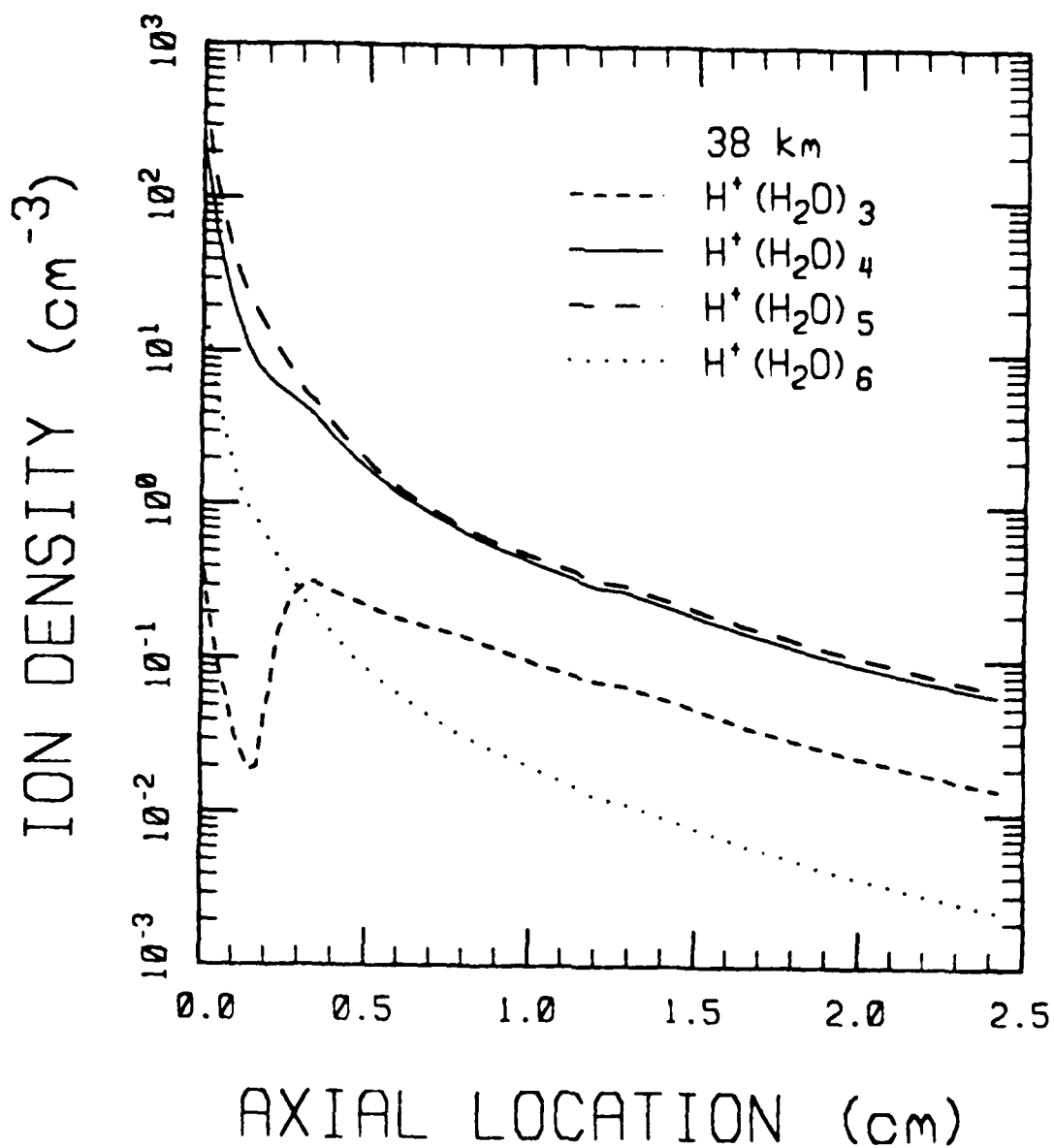


Figure 12. The Axial Dependence of Ion Cluster Number Density for the 38 Km Test Case.

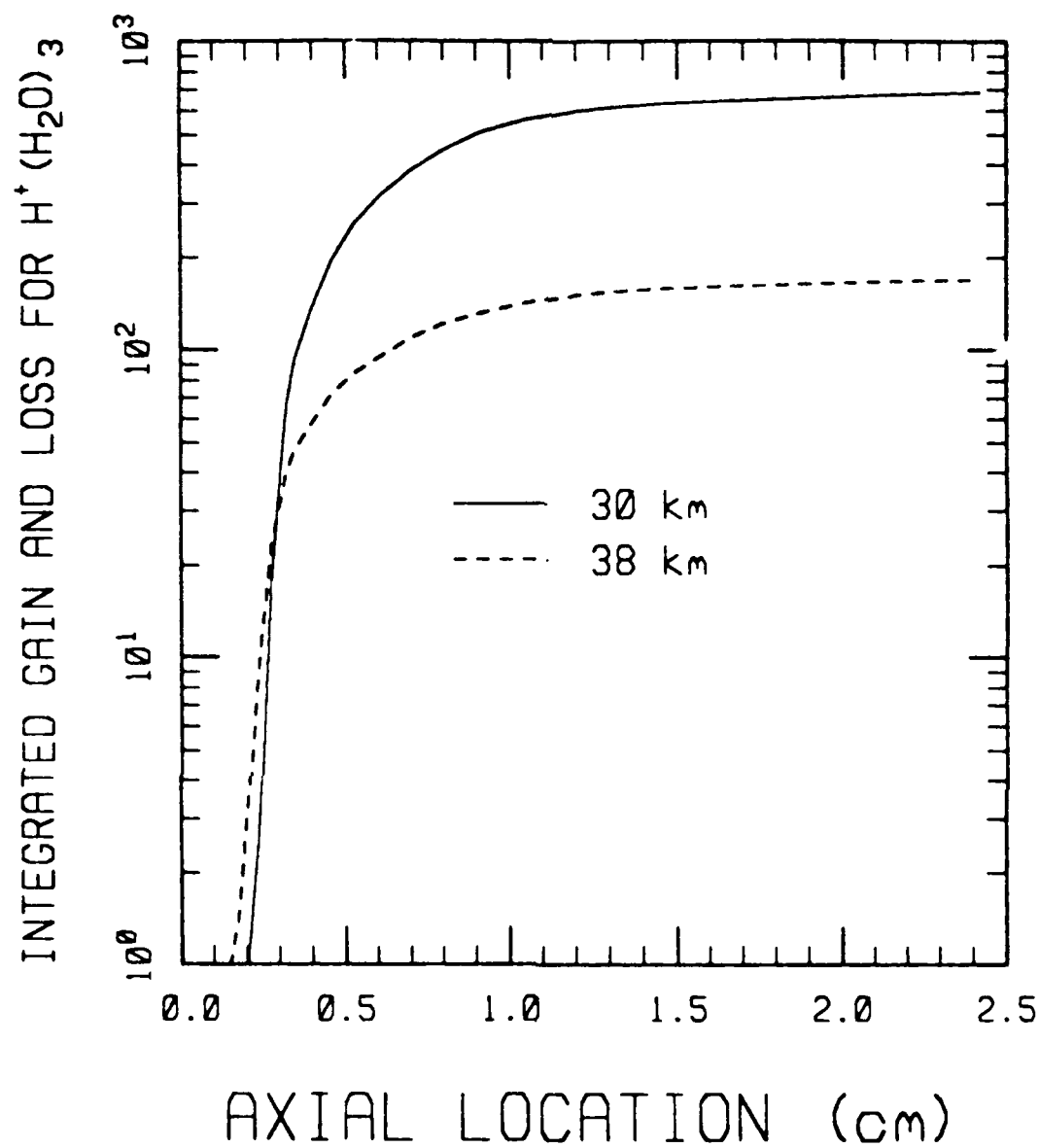


Figure 13. The Total Calculated Effect of Fragmentation and Agglomeration on the $H^+(H_2O)_3$ Number Density as a Function of Axial Position for the Two Test Cases.

simulation, since no $H^+(H_2O)_2$ clusters were carried in the solution. This process would not have a substantial effect on the conclusion, however, since at most 50% or so of the $H^+(H_2O)_3$ clusters would fragment. This would still leave their density almost two orders of magnitude above what it would be without the influence of fragmenting $H^+(H_2O)_4$ clusters.)

Figures 14 and 15 show the analogous plots for $H^+(H_2O)_4$ and $H^+(H_2O)_5$. In the former case the net effect of fragmentation is about a 10-20% increase in number density and in the latter case it is a decrease consistent with Figs. 9 and 10. This is because the density of $H^+(H_2O)_6$ clusters is quite low, so there is no significant source term for $H^+(H_2O)_5$.

6.4 Discussion

Any conclusion from these calculations is, of course, provisional in the absence of experimental verification. On the basis of these calculations, however, the two major conclusions are evident:

- 1) Agglomeration of additional water molecules onto ionic clusters does not seem to be a significant problem in mass spectrometric sampling of stratospheric ion clusters. This is primarily due to the low concentration of H_2O .
- 2) Fragmentation of clusters can be a significant problem. It is expected that a significant fraction of the incoming clusters will undergo fragmenting for the experimental conditions outlined here. For clusters such as $H^+(H_2O)_3$, where there are many initial clusters with more water molecules, the source due to the fragmentation of larger clusters can overwhelm the original population.

Although resources did not allow further investigation, it is quite possible that modifications in the experimental design could provide less severe fragmentation. Clearly, a lowering of the electric field strength would produce this result, but it would be at the cost of signal strength. Another solution is suggested by looking at Figs. 6 and 11. It can be seen

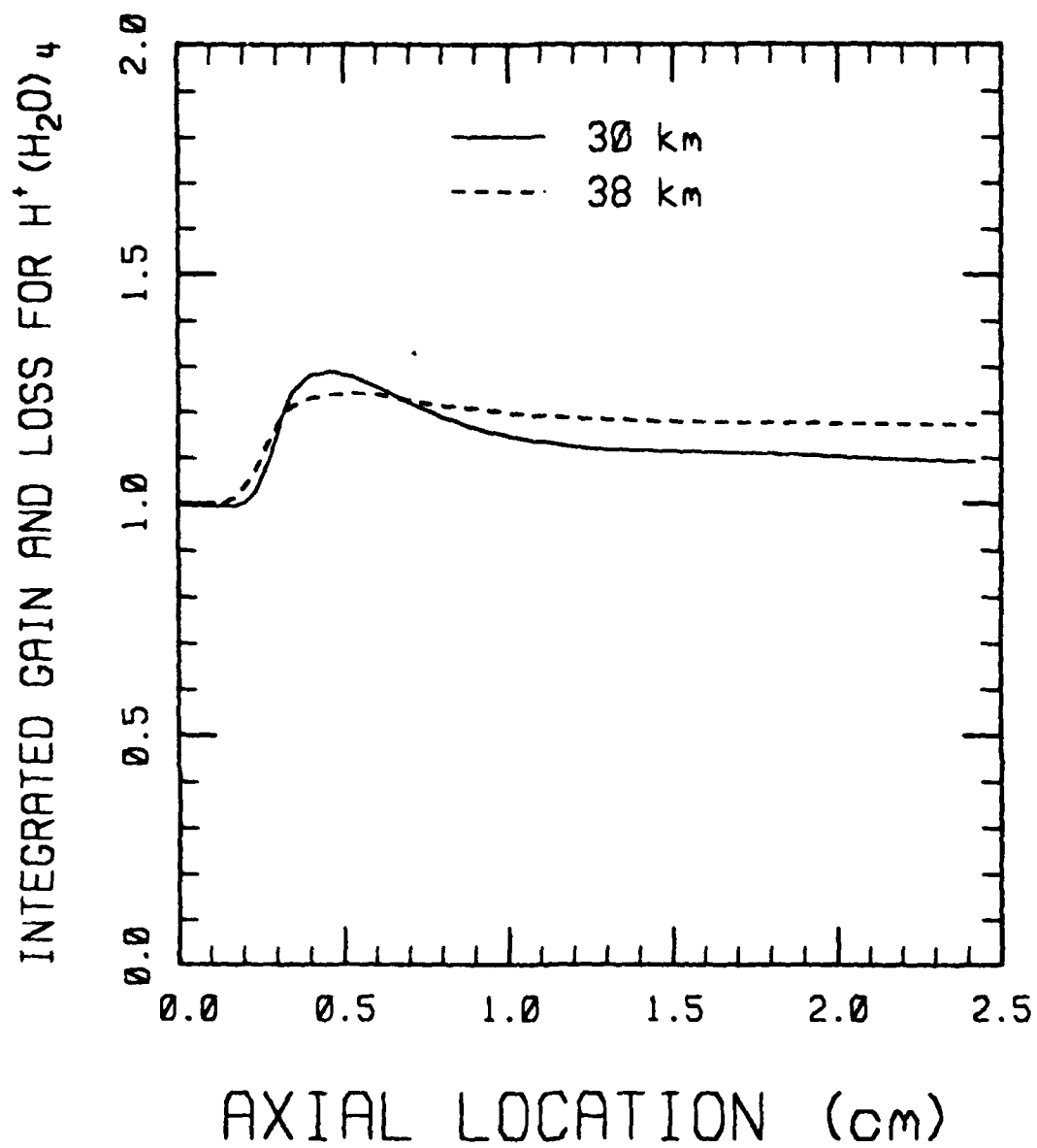


Figure 14. The Total Calculated Effect of Fragmentation and Agglomeration on the $H^+(H_2O)_4$ Number Density as a Function of Axial Position for the Two Test Cases.

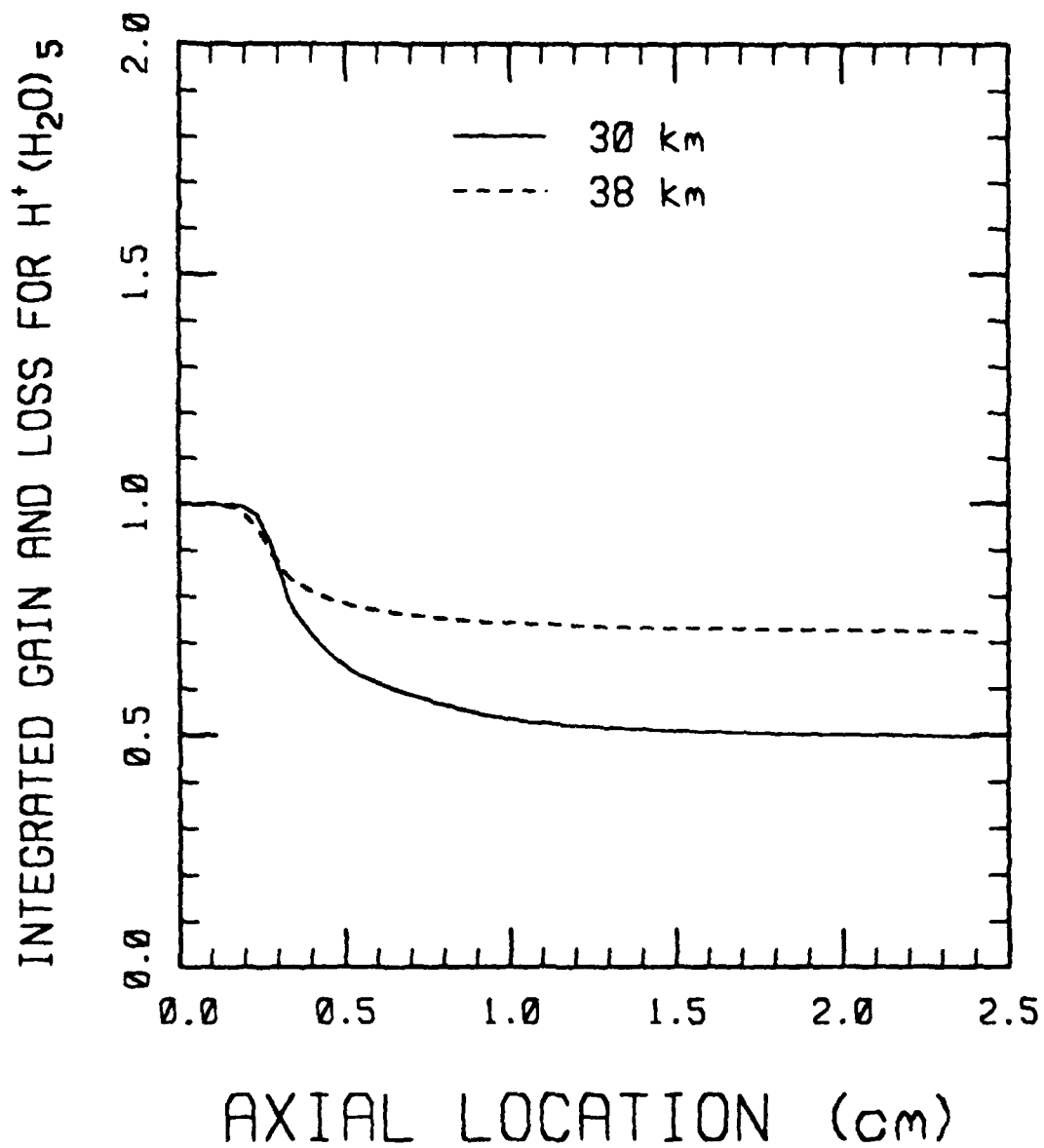


Figure 15. The Total Calculated Effect of Fragmentation and Agglomeration on the $H^+(H_2O)_5$ Number Density as a Function of Axial Position for the Two Test Cases.

that fragmentation is predicted to have its largest effect relatively near the orifice where the collision frequency is largest. Figure 6 predicts, for instance, that by about 0.7 cm from the orifice the fragmentation rate is an order of magnitude down from its peak. It is likely that potential grids placed beyond this point would produce substantially less fragmentation while maintaining a reasonable signal strength.

REFERENCES

1. Bird, G. A., Molecular Gas Dynamics, Clarendon Press, Oxford, 1976.
2. Elgin, J. B., "Monte Carlo Calculations of Mass Spectrometer Flow", Report AFGL-TR-83-0057, Air Force Geophysics Laboratory, February 1983. ADA128069
3. Shapiro, A.H., The Dynamics and Thermodynamics of Compressible Fluid Flow, the Ronald Press Co., New York, 1953, pp. 73-105.
4. Sharafudinov, R.G. and Skovorodko, P.A., "Rotational Level Population Kinetics in Nitrogen Freejets," Proceedings of the 12th International Symposium on Rarefied Gas Dynamics, AIAA Press, 1980.
5. Bird, G.A., "Breakdown of Continuum Flow in Freejets and Rocket Plumes," Proceedings of the 12th International Symposium on Rarefied Gas Dynamics, AIAA Press, 1980.
6. Liepmann, H.W., "Gaskinetics and Gasdynamics of Orifice Flow," Journal of Fluid Mechanics, Vol. 10, No. 5, 1961, pp. 65-79.
7. Smetana, F.O., Sherrill, W.A., and Schort, D.R., "Measurements of the Discharge Characteristics of Sharp-edged and Round-edged Orifices in the Transition Regime," Proceedings of the 5'th Rarefied Gas Dynamics Symposium, Vol. 2, Academic Press, 1967.
8. Labowski, M. Ryali, S., and Fenn, J.B., "Flowfield Calculations in Nonequilibrium Freejets by the Method of Characteristics," Proceedings of the 12th International Symposium on Rarefied Gas Dynamics, AIAA Press, 1980.
9. Bird, G.A., "Breakdown of Translational and Rotational Equilibrium in Gaseous Expansions," AIAA Journal, Vol. 8, No. 11, November 1970, pp. 1997-2003.
10. Bird, G. A., "Monte-Carlo Simulation in an Engineering Context", Proceedings of the 12th International Symposium on Rarefied Gas Dynamics, Vol. 74, Progress in Astronautics and Aeronautics, AIAA, New York, 1981.
11. Vincenti, Walter G., and Kruger, Charles H., Jr., Introduction to Physical Gas Dynamics, John Wiley and Sons, 1965, pp. 348-356.

12. Borgnakke, Claus, and Larsen, Paul S., "Statistical Collision Model for Monte Carlo Simulation of Polyatomic Gas Mixture", Journal of Computational Physics, Vol. 18, 1975, pp. 405-420.
13. Arnold, F., Henschen, G., and Ferguson, E. E., "Mass Spectrometric Measurements of Fractional Ion Abundances in the Stratosphere-Positive Ions," Planet. Space Sci. 29(1981), pp. 185-193.
14. Good, A., Durden, D. A., and Kebarle, P., "Ion Molecule Reactions in Pure Nitrogen and Nitrogen Containing Traces of Water at Total Pressures 0.5-4 torr. Kinetics of Clustering Reactions Forming $H^+(H_2O)_n$," J. Chem. Phys. 52(1970), pp. 212-221.
15. Good, A., Durden, D. A., and Kebarle, P., "Mechanism and Rate Constants of Ion-Molecule Reactions Leading to Formation of $H^+(H_2O)_n$ in Moist Oxygen and Air," J. Chem. Phys. 52(1970), pp. 222-229.
16. Lau, Y. K., Ikuta, S., and Kebarle, P., "Thermodynamics and Kinetics of the Gas-Phase Reactions: $H_3O^+(H_2O)_{n-1} + H_2O \rightleftharpoons H_3O^+(H_2O)_n$," J. Am. Chem. Soc. 104(1982), pp. 1463-1469.
17. See, for example, Forst, W., Theory of Unimolecular Reactions (Academic Press, N.Y., 1973).
18. Brady, J. W., Doll, J. D., and Thompson, D. L., J. Chem. Phys. 73(1980), pp. 2767-2772.
19. Castleman, A. W., "Nucleation and Molecular Clustering About Ions," Advances in Colloid and Interface Science 10(1979), pp. 73-128, and references therein.
20. Hsieh, E. T. -Y. and Castleman, A. W., "A Reconsideration of the Theory of Capture Cross Sections for Ion/Molecule Reactions and a Total Energy and Angular Momentum Conserved Average Charge-Dipole Interaction Theory," International Journal of Mass Spectrometry and Ion Physics 40(1981), pp. 295-329.
21. Su, T. and Bowers, M. T., J. Chem. Phys. 58(1973), pp. 3027-3037. See Ref. 20 for criticism and corrections concerning this approach.
22. Deguchi, S. and Muhleman, D. O., "Mesospheric Water Vapor", Journal of Geophysical Research, 87(C2), Feb. 20, 1982, pp. 1343-1346.
23. Kebarle, P., Annual Review of Physical Chemistry, 28, 1977, p. 445.

24. Ballanthin, J., Private Communication.

25. Handbook of Chemistry and Physics, 55th Edition, CRC Press, pp. F58.

END

DTIC

7-86